Bonnet Carré Spillway freshwater transport and corresponding biochemical properties in the Mississippi Bight

Sabrina Parra, Virginie Sanial, Adam Boyette, M. Kemal Cambazoglu, Inia Soto, Adam Greer, Luciano Chiaverano, Angie Hoover, Michael Dinniman

Parra, S.M., Sanial, V., Boyette, A.D., Cambazoglu, M.K., Soto, I.M., Greer, A.T., Chiaverano, L.M., Hoover, A., Dinniman, M.S., 2020. Bonnet Carré Spillway freshwater transport and corresponding biochemical properties in the Mississippi Bight. Continental Shelf Research 199, 104114. https://doi.org/10.1016/j.csr.2020.104114

Bonnet Carré Spillway freshwater transport and corresponding biochemical properties in the Mississippi Bight

Sabrina M. Parra [a,*,1], Virginie Sanial [b,3], Adam D. Boyette [b,4], M. Kemal Cambazoglu [b], Inia M. Soto [b,2], Adam T. Greer [b,5], Luciano M. Chiaverano [c], Angie Hoover [c], Michael S. Dinniman [d]

[a] American Society for Engineering Education at the US Naval Research Laboratory, Stennis Space Center, MS, USA
[b] Division of Marine Science, School of Ocean Science and Engineering, The University of Southern Mississippi, Stennis Space Center, MS, USA
[c] Division of Coastal Sciences, School of Ocean Science and Engineering, The University of Southern Mississippi, Ocean Springs, MS, USA
[d] Center for Coastal Physical Oceanography, Old Dominion University, Norfolk, VA, USA

ARTICLE INFO

Keywords:
Bonnet carré spillway
Mississippi river
Mississippi bight
Gulf of Mexico
River flooding
Shelf circulation
Planktonic communities

ABSTRACT

Large freshwater pulses to coastal ecosystems change local hydrologic regimes and alter biogeochemical processes. The Mississippi Bight coastal ecosystem, located in the northern Gulf of Mexico shelf, is influenced by extensive freshwater inputs: the Mississippi River (MSR) and several smaller rivers to the east. Under river flood conditions, MSR waters flow through the Bonnet Carré Spillway (BCS) to relieve pressure on levees in New Orleans, Louisiana. In 2015, mild wintertime temperatures and heavy rainfall throughout the MSR watershed led to extreme flooding and prompted an unusually early BCS opening on January 10, 2016 for 23 days. This study examines the effects of such intermittent freshwater diversions on local shelf circulation, planktonic distributions, and potential contaminant transport pathways. Physical, chemical, and remote sensing data collected one month after the BCS opening suggested the region was comprised of three water masses: shelf saltwater, MSR waters, and local river waters. Observations and circulation model results showed the BCS waters remained within the estuarine lakes and sounds, where winter wind patterns mixed the waters and prevented BCS waters from flowing onto the shelf. Freshwater within the Mississippi Bight was primarily from concurrent flooding of local rivers. Two distinct clusters of microplankton (offshore versus nearshore stations) and zooplankton (Chandeleur Sound versus other stations) community compositions were detected. No algal blooms were observed during this BCS opening. The 2016 wintertime BCS opening resulted in muted effects on the sounds and shelf because of its short duration and uncharacteristically early release.

1. Introduction

River diversions and spillway openings are common water management practices for alleviating rising river waters, and can result in large freshwater pulses that may have downstream biogeochemical effects depending on the volume of water, nutrient and sediment content, and where the water is transported. The Mississippi Bight, which is located within the northern Gulf of Mexico, is a managed coastal ecosystem that includes the heavily managed Mississippi River (MSR) with levees and dams all along its extent (Templet and Meyer-Arendt 1988; Kesel, 1988; Mossa 1996). The levees and dams control water, sediment, and nutrient fluxes down the river and into the Gulf. The strong confinement of the river leads to a control on the discharge, which becomes problematic during uncharacteristic spring floods. River floods require additional management when river discharges exceed design criteria for the levees. In the case of the MSR levees along New

* Corresponding author.
E-mail address: Sabrina.Parra@jhuapl.edu (S.M. Parra).
[1] Present address at Johns Hopkins University, Laurel, MD, USA.
[2] Present address at Universities Space Research Association, NASA Goddard, College Park, MD, USA.
[3] Present address at Université de Toulon, Toulon, France.
[4] Present address at Naval Oceanographic Office, Stennis Space Center, MS, USA.
[5] Present address at University of Georgia, Skidaway Institute of Oceanography, Savannah, GA, USA.

Orleans, Louisiana, the Bonnet Carré Spillway (BCS) was designed to protect the city.

The BCS is located ~52 km upriver from New Orleans (Fig. 1). This spillway allows floodwaters to flow from the MSR into the Lake Pontchartrain Estuary, which is connected to the Gulf of Mexico through the Lake Borgne Estuary (Fig. 1). The BCS has opened 14 times between its construction in 1931 and 2019, usually occurring in the spring months. However, the BCS opening of 2016 occurred in January, the earliest ever recorded. December 2015 was the warmest month for the continental US since record keeping began in 1895, likely caused by one of the strongest El Niño events on record (NOAA 2016). The unusually early BCS opening in January 2016 stemmed from two snow/melting events occurring within the extensive MSR watershed. First, two early-season winter storms during November 19–24, 2015 deposited 100–450 mm of snow over a wide region from South Dakota through northern Iowa/Minnesota to northern Illinois and Wisconsin (Santorelli 2016). Much of this snowpack melted within days, quickly filling rivers and tributaries. Second, two Midwest snow/rain events occurred in December (days 12–14 and 27–29). New snowpack delivered on December 12–14 over the northern Midwest (Rubin-Oster 2017) was melted by a rain event on December 27–29 with record totals of 250 mm in a 36-h period, which resulted in extensive flooding along the MSR (Holmes et al., 2016; Kong 2017).

At the same time, flooding was also experienced in the watersheds east of the MSR spanning parts of Mississippi, Alabama, and Georgia caused by extreme rainfall on December 21–28, 2015. Alabama received the brunt of that rainfall, with a local maximum of more than 350 mm (Huffman 2017). This regional flooding led to large freshwater discharges into the Mississippi Bight from a variety of local rivers, especially from the Mobile Bay watershed.

Periodic openings of the BCS introduce significant amounts of freshwater, inorganic nutrients, and organic matter that alter the physical, biological, and chemical properties of local coastal waters within Lake Pontchartrain Estuary and beyond (Mize and Demcheck, 2009; Lane et al. 2001; Bargu et al. 2011; Roy and White, 2012; Kolic et al. 2014; Adebayo and Amer, 2017; Roy et al. 2017). These nutrients can alter local trophic systems based on the amount and type of phytoplankton that become dominant (Officer and Ryther 1980; Turner et al. 1998). Additionally, it is well documented that large shifts in nutrient stoichiometry can promote the proliferation of potentially harmful algae (Dortch et al. 1998; Brammer et al. 2007).

Furthermore, freshwater input alters the physical properties of the water column, which can shift the community structure based on the temperature and salinity tolerances of different species (Barletta et al. 2005). This freshwater lens can also increase stratification of the shelf waters that leads to bottom water hypoxia, when combined with exponential growth, reproduction, and decomposition of phytoplankton due to an influx of nutrients (Rabalais et al. 2002; Dzwonkowski et al. 2018a; Haywood et al. 2018). Bottom water hypoxia also alters community structure in two main ways (1) more motile organisms (e.g. adult fishes, shrimp): flee, and (2) less motile organisms (e.g. larval fishes, oysters) experience physiological stress or even perish, resulting in “dead zones” (Marcus 2001; Purcell et al. 2001; Breitburg 2002). The western Mississippi Bight is subject to severe summertime hypoxia, including a large summertime hypoxic event that was observed in 2008 three months after a BCS opening that year (Brunner et al. 2008; Gundersen et al., 2019). The implications for these hypoxic events are that large intermittent events of freshwater carrying organic matter and nutrients may shift coastal ecosystems. However, the effects of the BCS discharge on the ecology and biogeochemistry of the sounds and shelf are not widely understood, especially in the wintertime.

Here, we focus on characterizing physical, biological, and chemical properties within the Mississippi Bight after the opening of the BCS in January 2016. The primary objectives of the current study were to characterize the physical, optical, and biogeochemical properties of coastal waters; and quantify phytoplankton and zooplankton abundance and composition. A vast array of measurements and model results were utilized to address these two objectives, including a combination of in situ, remote sensing and ocean modeling technologies. A three-day field cruise collected data throughout the western Mississippi Bight that

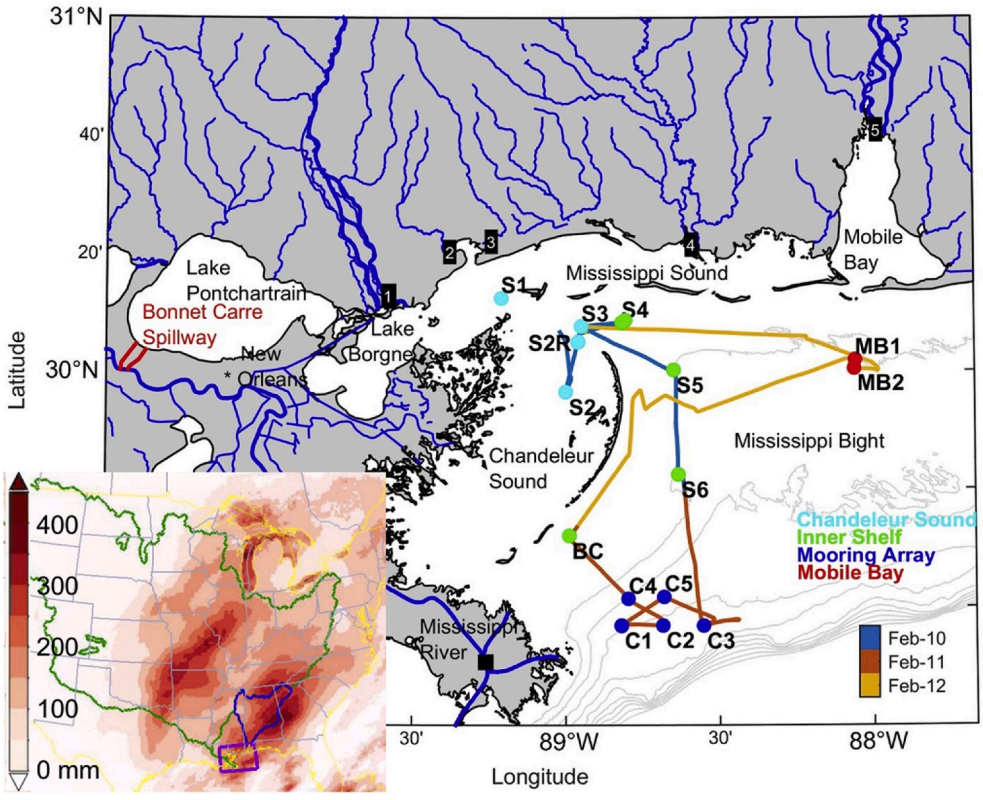

Fig. 1. Map of the Mississippi Bight with the cruise track, stations, and minor (thinner blue lines) and major (bold blue lines) rivers. Gray bathymetric contours are spaced every 20 m. Station colors represent different region designation. NOAA weather station PILL1 (black square) is at the end of the Mississippi River Birdfoot Delta. The red lines connecting the Mississippi River with Lake Pontchartrain Estuary shows the borders of the Bonnet Carré Spillway (BCS). Local rivers are numbered as follows: (1) Pearl, (2) Jordan, (3) Wolf, (4) Pascagoula, and (5) Mobile rivers. The inset map of the continental US shows the highlighted watersheds for the Mississippi River (green outline), and Mobile Bay (blue), the Mississippi Bight (purple) and with filled red contours of accumulated precipitation for December 2015 (mm, see color bar to the left). The yellow and gray contour represent country and state borders, respectively. (For interpretation of the references to color in this figure legend, the reader is referred to the Web version of this article.)

included hydrographic and biological sampling, optics, and water chemistry. Remote sensing products helped track the progression of the BCS waters. Physical oceanographic conditions were simulated using a high-resolution hindcast model of the Mississippi Bight following the BCS opening.

2. Data and methods

2.1. Study area

The Mississippi Bight (Fig. 1) is a pulsed river-dominated ecosystem located in the northern Gulf of Mexico shelf, east of the MSR Delta. The Mississippi Bight is affected by three main freshwater sources: the MSR, local rivers from Alabama and Mississippi, and the intermittent opening of the BCS via the Lake Pontchartrain Estuary (Fig. 1; Dortch et al. 2007), which provides an alternative pathway for MSR waters.

The MSR system is the dominant source of freshwater input into the Mississippi Bight, with a watershed draining approximately 41% of the continental United States (US; Fig. 1). The mean discharge from the MSR is ~17,000 m^3 s^{-1}, of which 70% traverses through the MSR Birdfoot Delta and the remaining 30% through the Atchafalaya River (Walker et al. 2005). While most of this freshwater is discharged onto the Louisiana shelf (westward), seasonal wind shifts to northward during the summer can push the river plume eastward into the Mississippi Bight (Morey et al. 2003; Schiller et al. 2011).

The local rivers east of the MSR Delta are dominated by the Mobile Bay discharge, which is the second largest freshwater source (~1700 m^3 s^{-1}) into the Gulf of Mexico after the Mississippi-Atchafalaya River System and ranks 5th among rivers in the United States (Dzwonkowski et al. 2011). Other local rivers flowing into the Mississippi Bight include the Pascagoula, Pearl, Jourdan, and Wolf rivers (Fig. 1).

The Mississippi Bight is subject to intense freshwater inflows during the spring freshet, intermittent tropical storms in the summer, and a drier season in late autumn to early winter. The spatial and temporal hydrographic variability in this system is driven primarily by winds and freshwater discharges (Stumpf et al. 1993; Walker et al. 2005), and, to a lesser extent, differential heating and cooling of surface waters (Schiller et al., 2011). Tides are microtidal in scale (mean tidal range is 30 cm) and are relatively weak in this region (Walker et al. 2005). Seasonal winds present two main patterns with relatively strong southward winds from passing cold fronts primarily in winter and spring, while summer and fall are relatively calm with weaker northward winds. Thus, circulation processes of the MSR plume and inner shelf waters are primarily driven by the seasonality of wind patterns (Walker et al. 2005; Cambazoglu et al. 2017). Circulation within this system is regulated by stratification that promotes wind-driven coastal Ekman transport (Dzwonkowski et al. 2011). These physical interactions are important for generating wind- and buoyancy-driven flows that ultimately influence the structure of regional food webs.

2.2. Strategy

Scientists led an interdisciplinary research effort to address key ecological and biogeochemical questions regarding the impact of a large freshwater plume within the Mississippi Bight during this unusual wintertime opening event. This effort was led by the CONsortium for oil spill exposure pathways in COastal River-Dominated Ecosystems (CONCORDE), a Gulf of Mexico Research Initiative (GoMRI) consortium aimed at describing fine scale ecosystem processes in river-dominated shelf waters (Greer et al. 2018).

2.3. Multidisciplinary datasets and analysis

To characterize the physical, bio-optical, and biogeochemical structure of the Mississippi Bight, a combination of in situ, remote sensing and ocean modeling technologies were deployed before, during and after a three-day (February 10–12, 2016) cruise on the research vessel (R/V) Point Sur. The cruise tracked the spatial distribution of the Mississippi Bight waters using continuous measurements of the near-surface conditions with a ship flow-through system (Fig. 1). Sampling stations were determined adaptively, measuring hydrography, optics, water chemistry, and biology with an integrated optics package, a rosette of 12 L Niskin bottles, a trace metal clean sampling system (acid-cleaned polyethylene bottle attached to a metal-free submerged rod), and a bongo net sampling system. A mooring array located near the MSR Birdfoot Delta (Fig. 1) measured current profiles before, during, and after the BCS opening. Satellite ocean color imagery described the surface conditions before, during, and after the cruise. Additionally, a high-resolution circulation model was used to examine the impact of buoyant freshwater plumes on the circulation in the Bight.

2.3.1. Bonnet Carré Spillway discharges

The US Army Corps of Engineers (USACE) operates the BCS under flood conditions to maintain the MSR at New Orleans below the levees' design flow rate of 35,400 m^3 s^{-1}. The Spillway is composed of 350 floodgates that are opened as needed, with a design discharge capacity of 7080 m^3 s^{-1}. Discharge is estimated daily, based on the number of opened gates and stage of the river at the spillway. Discharge rates for the different BCS openings were obtained from a variety of sources, as described in Table 1. The Spillway has opened 14 times since it was built in 1931 (as of August 2019) between January and July (Fig. 2 and Table 1). The discharge volumes for each opening have totaled between 2.1 and 30.1 km^3 with openings lasting between 13 (in 1975) and 79 days (second opening in 2019; USACE 2019). The BCS has been opened on average every 6 years; however, it has opened four times between 2016 and 2019, for the first time in consecutive years between 2018 and

Table 1
Bonnet Carré Spillway opening dates, duration, percent of bays opened, estimated total discharge from U.S. Army Corps of Engineers (USACE), and the percent volume of the total BCS discharge relative to Lake Pontchartrain Estuary total volume. Average total discharge for a BCS opening was 14.7 km^3 across all openings.

Year	Open and Close Dates (duration in days)	% Bays Opened	Estimated Total Discharge (km^3)	Lake Volume Percentage	Data Source
1937	Jan 28 - Mar 16 (48)	81%	15.2	238%	War Department (1937)
1945	Mar 23 - May 18 (57)	100%	30.1	470%	USACE (1945)
1950	Feb 10 - Mar 19 (38)	100%	13.4	209%	USACE (1950)
1973	Apr 8 - Jun 21 (75)	100%	23.5	367%	USACE (1974)
1975	Apr 14 - Apr 26 (13)	64%	2.11	33%	USACE (1975)
1979	Apr 17 - May 31 (45)	100%	13.9	217%	USACE (1980)
1983	May 20 - Jun 23 (35)	100%	15.2	238%	USACE (1984)
1997	Mar 17 - Apr 17 (32)	85%	11.7	183%	Perret et al. (1997)
2008	Apr 11 - May 8 (28)	46%	7.5	117%	USACE (2019)
2011	May 9 - Jun 20 (43)	94%	21.9	342%	USACE (2019)
2016	**Jan 10 - Feb 1 (23)**	**60%**	**6.9**	**107%**	USACE (2019)
2018	Mar 8 - Mar 30 (23)	52%	5.8	91%	USACE (2019)
2019	Feb 27 - Apr 11 (44)	59%	15.1	236%	USACE (2019)
2019	May 10 - Jul 27 (79)	48%	23.0	360%	USACE (2019)

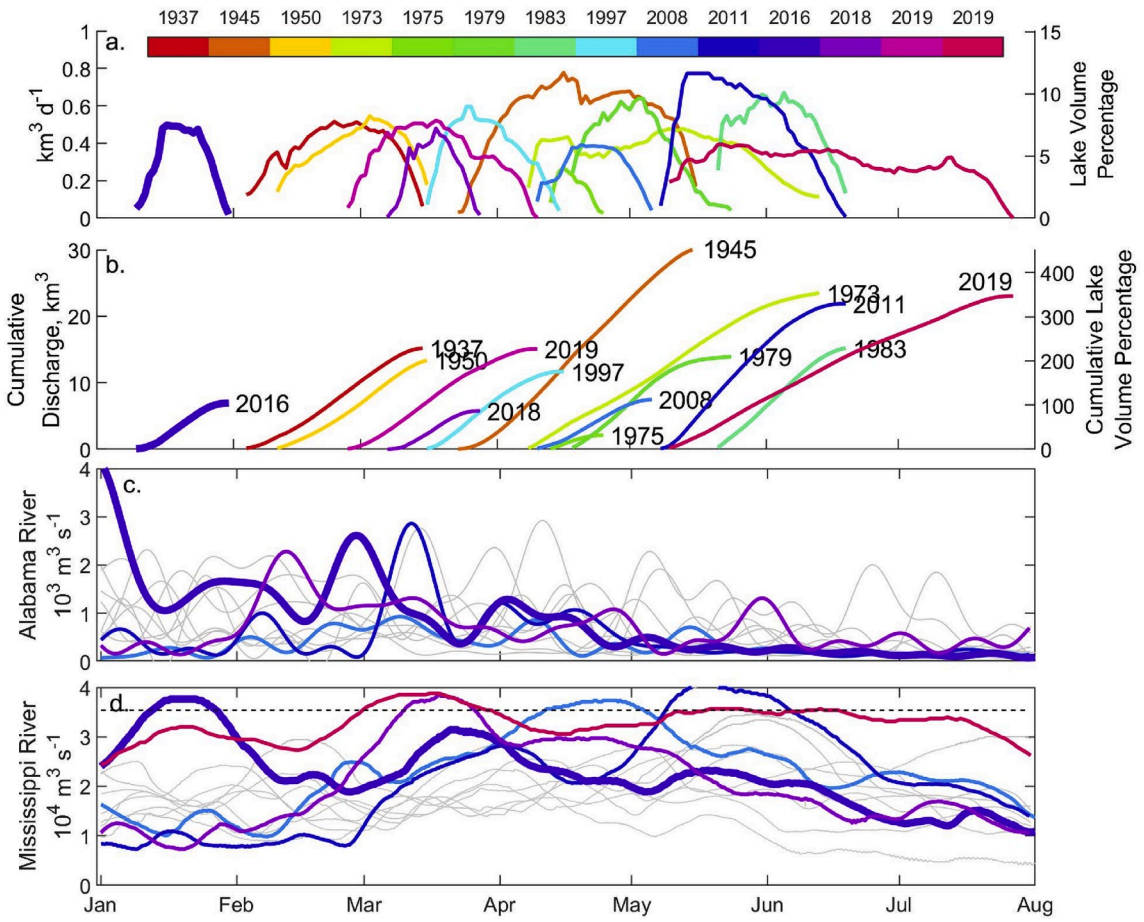

Fig. 2. Caption: Bonnet Carré Spillway (BCS) discharges. (a) The total daily discharge rates in $km^3\ d^{-1}$ (left y-axis) and percent of Lake Pontchartrain Estuary volume (right y-axis, lake volume of 6.4 km^3) of each spillway opening (see color bar for respective year) in their respective time of year. (b) The cumulative discharge (left y-axis) and cumulative lake volume (right y-axis) of each spillway opening in their respective time of year. The opening of 2016 is displayed in bold blueish-purple. Data obtained from US Army Corps of Engineers (USACE). More details regarding the different BCS openings available in Table 1. (c) Alabama River discharges as measured at Montgomery, AL for 2007 to 2018 from January through August. (d) Mississippi River discharge as measured at Baton Rouge for 2007–2019 from January through August, with the dashed black line representing the discharge that triggers a BCS opening (35,400 $m^3\ s^{-1}$). The colored lines in (c) and (d) match the colors for the 2008, 2011, 2016 and 2018 BCS openings in a) and b). The gray lines represent the other years. (For interpretation of the references to color in this figure legend, the reader is referred to the Web version of this article.)

2019, and for the first time twice in one year in 2019. The diverted waters flow through a 4.1 km wide and nearly 8.7 km long floodway before reaching Lake Pontchartrain Estuary (Fig. 1). Lake Pontchartrain Estuary has an estimated volume of 6.4 km^3 and is connected to the Gulf of Mexico through Lake Borgne Estuary (Fig. 1; Turner et al. 2004).

2.3.2. *River discharges*

In order to compare the relative discharges and flooding stage of local rivers and the MSR, we used the Alabama River as representative of local rivers (Dzwonkowski et al. 2018b). The river discharges were downloaded from US Geological Survey (USGS) National Water Information System (https://waterdata.usgs.gov/nwis/sw). The MSR discharge at Baton Rouge, LA and the Alabama River discharge at Montgomery, AL from January to July are presented in Fig. 2c and d for the period 2007–2019 for comparison with relevant BCS openings and discharges.

2.3.3. *CTD casts*

Conductivity-temperature-depth (CTD) casts were performed from near-surface (1–2 m deep) to near-bottom (within 1–3 m from the bottom). Depths ranged from <10 m within the Mississippi Sound to >60 m at the Mooring Array near the shelf slope (Fig. 1). CTD casts were performed at all stations except S2 (the southernmost station in Chandeleur Sound). Near-surface (1–3 m) seawater samples for dissolved oxygen (DO), inorganic nutrients, chlorophyll-a (chl-a), and phytoplankton image analysis were taken with 12 L Niskin bottles mounted on a CTD rosette.

2.3.4. *Biogeochemistry and trace metal data*

The waters from the MSR diverted through the BCS can be tracked through their chemical signature relative to local river sources. Differentiation of water sources was accomplished through examining a suite of tracers, in particular, isotopic oxygen composition ($\delta^{18}O$), and trace elements such as barium (Ba) and cesium (Cs). Isotopic oxygen composition represents the ultimate tracer for the origin of a freshwater source because it is part of the water itself (Wagner and Slowey, 2011). Barium is also commonly used as a freshwater tracer in the coastal ocean (Joung and Shiller 2014; Guay and Falkner 1997), and can be used to differentiate between different river sources depending on the relative occurrence of carbonate within the watersheds (Dalai et al. 2002). Oceanic concentrations of $\delta^{18}O$ (1.1‰; Wagner and Slowey, 2011), Ba (62 nM; Joung and Shiller 2013), and Cs (2.2 nM; Ho et al. 2019) differ from those of the MSR and local rivers (Hanor and Chan 1977; Joung and Shiller 2013), thus allowing the differentiation between the different water sources.

Surface (~0 m) water samples were collected at all stations using a

trace metal clean system consisting of a polyvinyl chloride (PVC) pole fitted with a Plexiglas bottle holder using narrow Tygon® tubing to capture the undisturbed surface thin layer of riverine freshwater (Shim et al. 2012; Joung and Shiller 2013). Additionally, riverine freshwater samples were collected using the same PVC pole during five field trips to the MSR and local rivers (Pascagoula, Mobile, Pearl, Jourdan, and Wolf rivers) conducted between October 2015 and June 2016. Both river and cruise samples were filtered immediately through 0.45 μm pore size polyethylene syringe filters. The samples for Cs and Ba analysis were acidified to a pH of 2 and stored for analysis in the laboratory. Approximately 100 mL of the filtrate was stored in pre-cleaned 125 mL amber polyethylene bottles and frozen for future analysis of dissolved inorganic nutrient concentrations (dissolved inorganic nitrogen (DIN) and phosphate, PO_4^{3-}) in the laboratory.

The Ba and Cs concentrations were analyzed with a high-resolution inductively-coupled plasma mass spectrometer. Barium concentrations were determined following an isotope dilution method (Joung and Shiller, 2014) and Cs concentrations by standard additions to a seawater sample (Shim et al. 2012). Dissolved inorganic nutrients were examined colorimetrically using a Skalar autoanalyzer (Liefer et al. 2013, 2014). Oxygen isotope $\delta^{18}O$ concentrations were determined using isotope ratio infrared spectroscopy (Picarro Inc.) following van Geldern and Barth (2012). More information on $\delta^{18}O$ data can be found in Sanial et al. (2019).

A simple mixing model was applied to salinity and $\delta^{18}O$ to estimate the concentrations of MSR waters throughout the sounds and shelf (Sanial et al. 2019). Briefly, a set of two linear equations describing the mixing between seawater, MSR waters, and local AL/MS river waters were used with the additional constraint that the sum of the contribution of these three different sources of water is equal to unity. The MSR fraction represents the fraction of MSR waters to the total freshwater (i.e., fractions of local river waters plus MSR waters). We estimated the MSR fraction only for stations with salinity <33 psμ because of increased uncertainties at higher salinities; therefore, it was not calculated at station S5. Differences in local river waters were not distinguished by their $\delta^{18}O$ signature because of the similar latitude of origin of water feeding the local rivers and similar topographies.

2.3.5. Plankton data

Near-surface water samples for chl-a and microplankton community composition were obtained from the Niskin bottles. Chl-a was determined following the method described by Welschmeyer (1994) and was analyzed on a Turner 10-AU fluorometer after the cruise. Aliquots (1 L) for microplankton imaging analysis were filtered through a 202 μm sieve prior to imaging.

FlowCAM® was used to image microplankton (<200 μm) size classes for community composition and particle concentration (particles L^{-1}) (Sieracki et al. 1998; Álvarez et al. 2014). Particles within 5.0 mL unconcentrated natural samples were imaged through a 10× objective and 100 μm flow cell using 'trigger mode' to image particles that contain photosynthetic pigments. Imaged particles were classified into four broad taxonomic categories: dinoflagellates, diatoms, other (chlorophytes, cryptophytes, and nanoflagellates, microzooplankton), and unidentified particles, which includes detrital material, plankton fragments (e.g. diatom frustules, crustacean appendages). Microplankton cell volume (i.e., biovolume) estimates were recorded by the FlowCAM using the area-based geometry (i.e. cylinder for diatoms, prolate spheroid for all other groups excluding unidentified particles) for each cell. Biovolumes provided a metric for the distribution of cell size classes and contribution to microplankton community composition, particularly for chain diatoms (Hillebrand et al. 1999).

Zooplankton was collected using a paired bongo net (60 cm in diameter) fitted with 202 μm and 333 μm mesh nets. Sampling took place at all stations except S3, S5, S6, C2, C4, and BC (Fig. 1). The paired bongo net was towed just below the water surface (~1 m) for a duration of 10 min at each station. Mechanical flowmeters attached to the opening of each net estimated the volume of filtered water. All samples were immediately preserved in 95% ethanol at sea and analyzed in the laboratory. Aliquots from each sample were taken following the method by Harris et al. (2000). Only zooplankton collected with the 333 μm-mesh net were analyzed for this study. For each sample aliquot, the zooplankton were enumerated and classified into 19 taxonomic categories. Zooplankton abundances were standardized by aliquot and filtered volumes to yield estimates of taxon-specific concentrations (individuals m^{-3}).

Several statistical techniques were used to describe the changes in abundance of plankton throughout the study area. Stations with plankton samples were first divided up into three different geographical areas, including the Chandeleur Sound, Mobile Bay, and Mooring Array. Cluster analysis (SIMPROF, explained below) and principal component analysis (PCA) were used to examine the similarities between stations based on community structure of plankton and physico-chemical variables. The PCA biplot visualized the relationships between station physical and chemical oceanographic data and microplankton biovolumes. Only stations with complete data (except S3 and C1) for microplankton and biogeochemistry were used in the PCA, which was implemented in R (v3.5.1) and visualized using the R package ggbiplot (Vu 2011).

To test for potential spatial structure in zooplankton community composition, a cluster analysis (group average) was performed including abundances of 19 different zooplankton taxa. Abundance data were fourth-root transformed, from which similarity matrices were constructed using the Bray-Curtis similarity index. A similarity profile (SIMPROF, 1000 permutations, $\alpha = 0.05$) was used to identify homogeneous clusters. An analysis of similarity (ANOSIM) was then performed to test for significant differences in zooplankton composition among clusters identified by the SIMPROF. A Similarity Percentage (SIMPER) analysis was then used to determine the contribution of each zooplankton taxa (%) to the total dissimilarity in community structure between clusters. These analyses were performed in Primer v6. In addition, differences in zooplankton concentration among different regions were tested for significance ($\alpha = 0.05$) by Kruskal-Wallis H test, and post-hoc pairwise comparisons. Kristal-Wallis test is a non-parametric method to assess the significant differences between different samples. The H test is significant when it exceeds the critical chi-square value, estimated from the degrees of freedom (df) and probability value (p).

2.3.6. Bio-optical data

Underway bio-optical data were collected to understand the effects of freshwater on the water clarity, particle concentration, and biological productivity in the region. Throughout the cruise, salinity, temperature, absorption, and attenuation were continuously collected from near-surface waters (~2 m) using the ship's flow-through system. The Sea-Bird spectral absorption and attenuation (ac-s) sensor measured total spectral absorption coefficient, $a_t(\lambda)$, and beam attenuation coefficient, $c_t(\lambda)$, for 390–700 nm wavelengths. The ac-s flow-through setup followed the protocol outlined by National Oceanic and Atmospheric Administration (NOAA) Technical Report NESDIS 146 (Ondrusek and Lance 2015). To ensure stability and reliability, the ac-s instrument was placed in a temperature-stabilized water bath to dissipate the heat generated by the instruments and maintain an instrument constant temperature. The ac-s was interfaced with a WETLabs® DH4 data logger with additional input from the vessel's flow-through dynamic positioning system, Sea-bird CTD, and fluorometer.

The ac-s instrument was calibrated prior to and after the cruise. Post processing of the ac-s data followed the methods defined by the WET-Labs protocols (WETLabs, 2011). First, the ac-s data were merged and binned at 1 s intervals with CTD data using WETLabs Archive Processing Software. Water absorption corrections for temperature and salinity were applied using the ship's flow-through data following techniques outlined by Pegau et al. (1997). The proportional scatter correction was

also applied to the ac-s data (Röttgers et al. 2013).

As a proxy for chl-a absorption and concentration, the absorption line height was calculated (ALH) following Roesler and Barnard (2013) by using the red peak of phytoplankton absorption near 676 nm. ALH was converted to chl-a units by direct comparison with discrete chl-a samples collected during the cruise ($y = 0.93x - 0.12$; $r^2 = 0.85$). The logarithmic absorption slope (400–450 nm) was used as a proxy for colored dissolved organic matter (CDOM) and detrital material. The ratio between ALH and spectral slope was used to determine regions where either CDOM or chl-a dominated the waters. The scattering coefficient at 685 nm ($c_t[685] - a_t[685]$) was used as a proxy for high sediment waters.

2.3.7. Mooring array data

The current patterns on the shelf near the MSR Delta between January and February 2016 were characterized by a set of five bottom moorings (C1–C5 in Fig. 1). Five upward-facing RD Instruments Workhorse acoustic Doppler current profilers (ADCPs) were moored ~21 km east of the MSR Delta (C1–C5 in Fig. 1; Parra et al. 2019). The deployment spanned from November 2, 2015 through April 13, 2016 using the trawl-resistant Barny Sentinel design (Perkins et al. 2000) for protection from extensive fishing and commercial boating activities of this region. Details pertaining to the instrument setup, deployment sites, and quality control of the data are found in Parra et al. (2019).

Current variability at the C1–C5 mooring locations (Fig. 1) was studied using an empirical orthogonal function (EOF) analysis. This technique extracts spatiotemporal patterns from the time series at multiple spatial points and separates that variability into orthogonal functions or modes (Emery and Thomson 2001). In other words, it can extract the main spatial patterns in the study region and describes intensity changes of the patterns over time. Each mode consists of a spatial structure and a representative temporal variability that represents a percent of the total variance observed, where the first few modes explain most of the variance. For example, mode 1 represents the spatial structure with the largest variability in the time series. Subsequent modes represent progressively smaller variability in the signal.

2.3.8. Wind observations

Hourly wind time series was obtained from the NOAA National Data Buoy Center Coastal-Marine Automated Network station PILL1 located on the southern edge of the MSR Delta (29.179° N, 89.259° W) (see Fig. 1). These hourly winds, measured at 9.5 m above sea level, were used in conjunction with the Mooring Array's current profiles to analyze the circulation.

2.3.9. Satellite-gauge precipitation

Accumulated precipitation estimates over the MSR and Mobile Bay watersheds were obtained for December 2015 from National Aeronautics and Space Administration's (NASA) Integrated Multi-satellite Retrievals for Global Precipitation Measurements, version 5, monthly Level 3 with 0.1° resolution (Huffman 2017). The precipitation estimates were plotted over the MSR and Mobile Bay watersheds for context, with watershed outlines obtained from USGS Elevation Derivatives for National Application Watershed Atlas (https://edna.usgs.gov/watersheds/kml_index.htm).

2.3.10. Ocean color satellite data

Ocean color satellite imagery provides a synoptic view of the region's surface conditions, setting the stage for the higher resolution measurements collected during the cruise. Satellite-derived chl-a estimates (mg m^{-3}) were obtained from the Moderate-Resolution Imaging Spectroradiometer (MODIS) onboard the Aqua satellite. The quality controlled MODIS-Aqua Level-3 chl-a monthly means and climatology were obtained from the NASA-Ocean Biology Processing Group website at 4-km spatial resolution. Chl-a is derived using a combination of the OC3 algorithm from O'Reilly et al. (1998) and the color index from Hu et al. (2012). February chl-a data were averaged over a 15-year period ranging from 2003 to 2017 to obtain the monthly climatology. This February climatology was then used to extract anomaly fields within the Mississippi Bight by subtracting the 15-year mean from the monthly means. Although a 15-year mean was used to create anomalies, we only show results from the last 9 years.

The spatial extent of surface bio-optical properties and freshwater discharge during the BCS opening and three-day research cruise was determined using satellite-derived particle backscattering at 551 nm (m^{-1}) from the Visual Infrared Imaging Radiometer Suite (VIIRS). It was obtained from the NOAA Comprehensive Large Array-data Stewardship System (CLASS) website (http://www.class.ngdc.noaa.gov/) and processed to Level 3 at 750m resolution using the Naval Research Laboratory's N2gen code based on NASA's L2gen software (Werdell et al. 2013) and standard atmospheric correction (Gordon and Wang, 1994). Standard flags were used to mask contamination from land, clouds, sun glint, and other potential disturbances to the radiance signal. Particle backscattering was derived using the Quasi-Analytical Algorithm (QAA, Lee et al. 2002, 2014). Useful remote sensing imagery of backscattering was available for 12 nonconsecutive days after the BCS opening in January 10 until the research cruise ended in February 12. Cloud cover or glare restricted use of the other days. High values indicate higher concentrations of suspended sediments/particles.

2.3.11. Hydrodynamic modeling

Two numerical models were used before, during, and after the cruise. Results from an hourly 1-km regional application of the Navy Coastal Ocean Model for Gulf of Mexico (NCOM-GOM; Jacobs et al. 2016) were initially used for cruise planning activities. Predicted water temperature, salinity, and currents were provided to the scientific crew of the research vessel on a daily basis. The model data were supplemented with the latest observed ocean color satellite data. The NCOM-GOM domain covered Lake Pontchartrain Estuary and incorporated the BCS opening in model simulations using actual daily discharge rates as reported by the USACE. The atmospheric forcing originated from the hourly ~17 km operational Coupled Ocean-Atmosphere Mesoscale Prediction System (COAMPS) and the tidal boundary conditions were generated from the global Oregon State University Tidal Inversion Software solution (OTIS) (Barron et al. 2006).

A higher spatial resolution (400-m) COAWST-based (Coupled Ocean Atmosphere Wave Sediment Transport modeling system; Warner et al. 2010) modeling framework was developed as the CONCORDE project's Synthesis model (Greer et al. 2018). The CONCORDE Synthesis model implemented the ocean circulation component by using the Regional Ocean Modeling System (ROMS; Shchepetkin and McWilliams, 2005; Haidvogel et al. 2008) as the modeling framework. The CONCORDE Synthesis model had 24 terrain-following vertical layers in the vertical. The atmospheric forcing was improved by using a higher spatial (~1 km) resolution product called the CONCORDE Meteorological Analysis (CMA; Fitzpatrick and Lau, 2018), which resolves mesoscale features as well as diurnal processes critical for capturing ocean dynamics near the ocean-land interface. The initial condition and lateral boundary forcing data, including tidal forcing, were obtained from NCOM-GOM. Observed river discharge from USGS data were used as river forcing. The western open boundary of the CONCORDE synthesis model is in the eastern side of Lake Pontchartrain Estuary. It received its open boundary forcing from NCOM-GOM output, including higher water levels in Lake Pontchartrain Estuary due to the BCS opening, which introduces the freshwater from Lake Pontchartrain Estuary into the western Mississippi Sound (Fig. 1). The open boundary forcing in Lake Pontchartrain Estuary was also corrected and enhanced by incorporating salinity measurements reported by the Lake Pontchartrain Basin Foundation (https://saveourlake.org/lpbf-programs/coastal/hydrocoast-maps/salinity/; Lopez et al. 2015). The CONCORDE synthesis model provides hourly salinity, temperature, and velocities before, during, and after the BCS opening (January 10-February 1, 2016) and the cruise (February 10–12,

2016). Nothing is passed from the CONCORDE model to the NCOM model. The CONCORDE model was created to generate higher resolution results in our area of interest and to embed an ecosystem model (not utilized in this work; Greer et al. 2018).

The CONCORDE Synthesis model was used to simulate drifter trajectories within the Mississippi Sound and Bight representing the advection and transport of different estuarine water masses after the opening of the spillway. Neutrally buoyant simulated drifters were periodically released at chosen locations. They were advected within the model code (not post-processed with saved velocities) at every model time step using the three dimensional advective velocity of the model (at the time and position of the tracer particle) plus a vertical diffusion term which was included by adding a random walk in the vertical direction (Hunter et al. 1993; Visser, 1997). Simulated drifter groups were released in multiple vertical layers every 10 days for seven months starting in mid-October 2015 and covering the spillway opening time frame from two different locations: at the mouth of Mobile Bay (8 simulated drifters) and inside Lake Pontchartrain Estuary (5 simulated drifters). For the Mobile Bay simulated drifters, four were released just north of the inlet and another four just south of the inlet.

To understand the effects of the BCS opening in the advection and transport of river water into the Mississippi Bight, the CONCORDE Synthesis model was run under two different conditions: with and without the BCS discharge. In these twin experiments, the western open boundary forcing at Lake Pontchartrain Estuary was the only difference, with all other conditions such as atmospheric forcing, southern open boundary condition, river forcing, etc. remaining the same. Particles were released as above (both before and after the spillway opening) for both scenarios.

3. Results

3.1. Bonnet Carré Spillway opening in January 2016

The 2016 opening spanned January 10 through February 1 (23 days). At its peak, 210 open gates resulted in a maximum discharge of 0.5 $km^3\ d^{-1}$, nearly 7% of the Lake Pontchartrain Estuary volume. The cumulative discharge volume of the entire 2016 opening was 6.9 km^3, representing 107% of the total volume of Lake Pontchartrain Estuary. Relative to other BCS openings, this was the third lowest cumulative discharge, ahead of 1975 and 2018, and the earliest opening as of the end of 2019.

Remote sensing optical backscatter indicated that the BCS plume hugged the southern coast of Lake Pontchartrain Estuary, and remained confined within the lake until after January 19 (Fig. 3). Winds to the south and west during those first nine days kept the plume within the lake. By January 29, the plume had expanded into Lake Borgne Estuary and the sounds, forced by an eastward wind. The relatively strong winds of February 4–5 mixed the plume and diluted its backscattering signal in the estuarine lakes and sounds. The plume finally expanded throughout Lake Pontchartrain Estuary on February 11–12 driven by northeastward winds that also pushed the plume remnants out to Lake Borgne Estuary and the Chandeleur Sound.

3.2. Context of the 2016 BCS opening

Fig. 4 shows the monthly chl-a anomalies for February from 2008 to 2016 relative to a 15 year monthly mean of February spanning from 2003 to 2017. In general, February anomalies tended to be negative or near zero (e.g., 2008, 2009, 2012, 2014, 2015). Two main exceptions include instances when the MSR intruded eastward (2011) and with strongly elevated anomalies in the Mobile Bay region and coastal waters (2010, 2013, 2016). February 2016 stands out as extremely anomalous

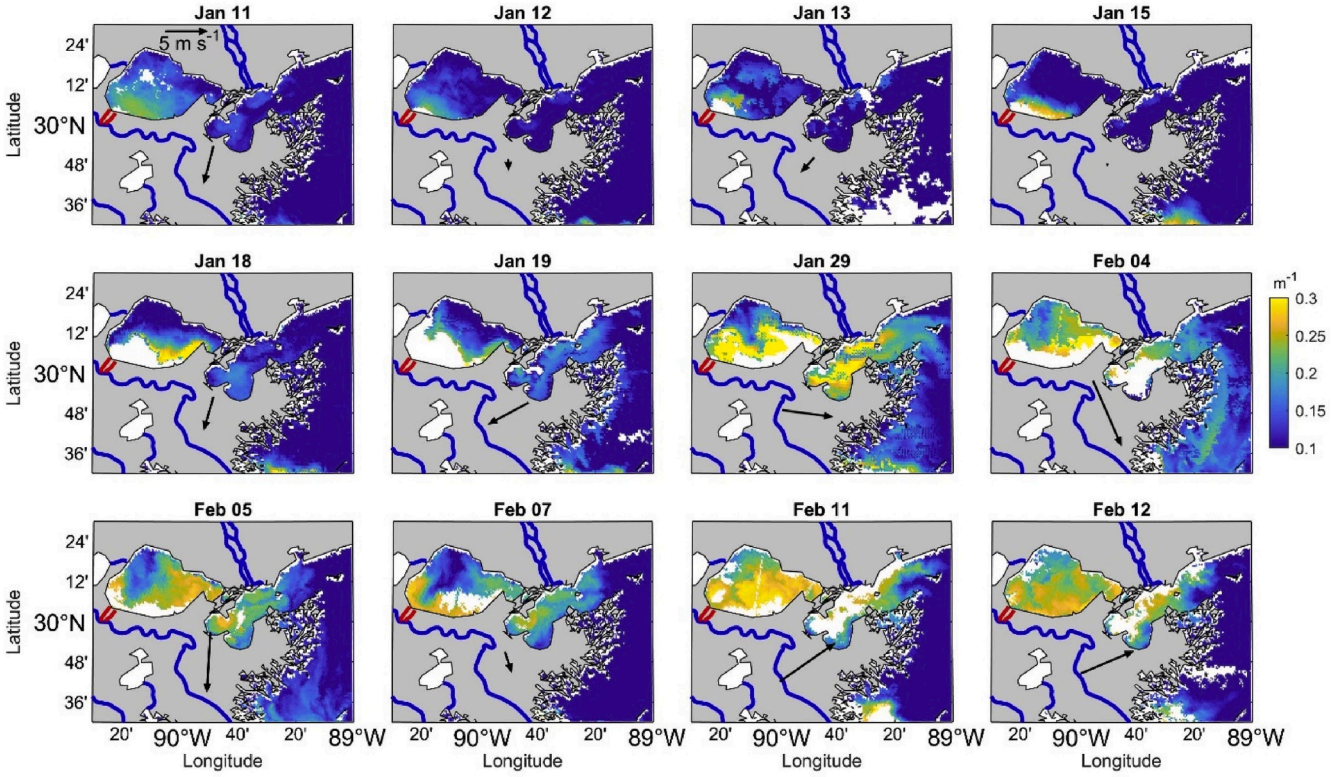

Fig. 3. Tracking the BCS plume with VIIRS satellite-derived particle backscattering at 551 nm in Lake Pontchartrain Estuary. Black vector represents mean wind speed and magnitude on remote sensing day. Blue lines represent rivers and red lines delineate the BCS spillway connecting MSR and Lake Pontchartrain Estuary (Fig. 1). (For interpretation of the references to color in this figure legend, the reader is referred to the Web version of this article.)

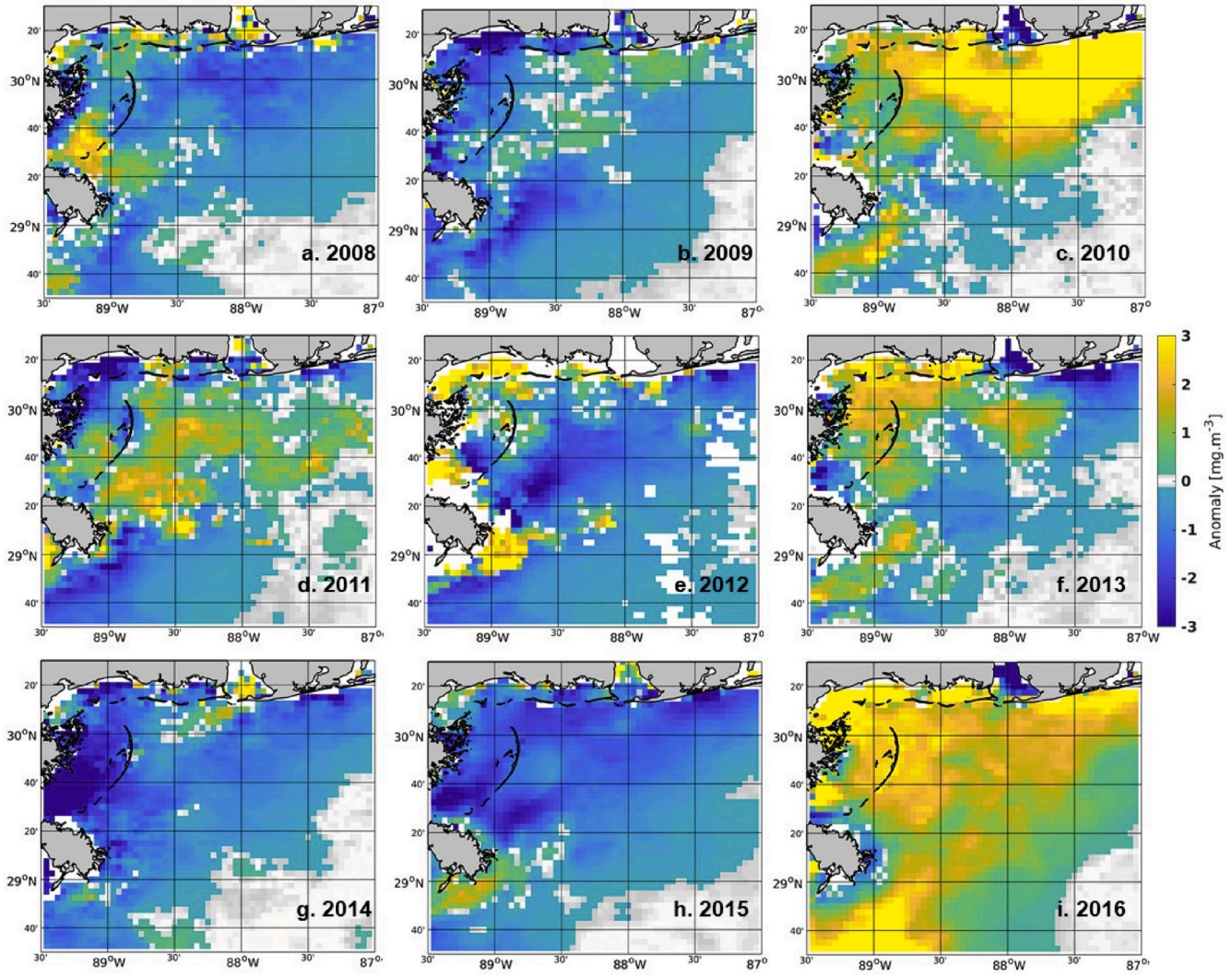

Fig. 4. MODIS-Aqua chl-a anomalies (mg m^{-3}) for February from 2003 to 2016. Blue colors represent lower and yellow higher chl-a values with respect to a 15-year chl-a climatology for February. (For interpretation of the references to color in this figure legend, the reader is referred to the Web version of this article.)

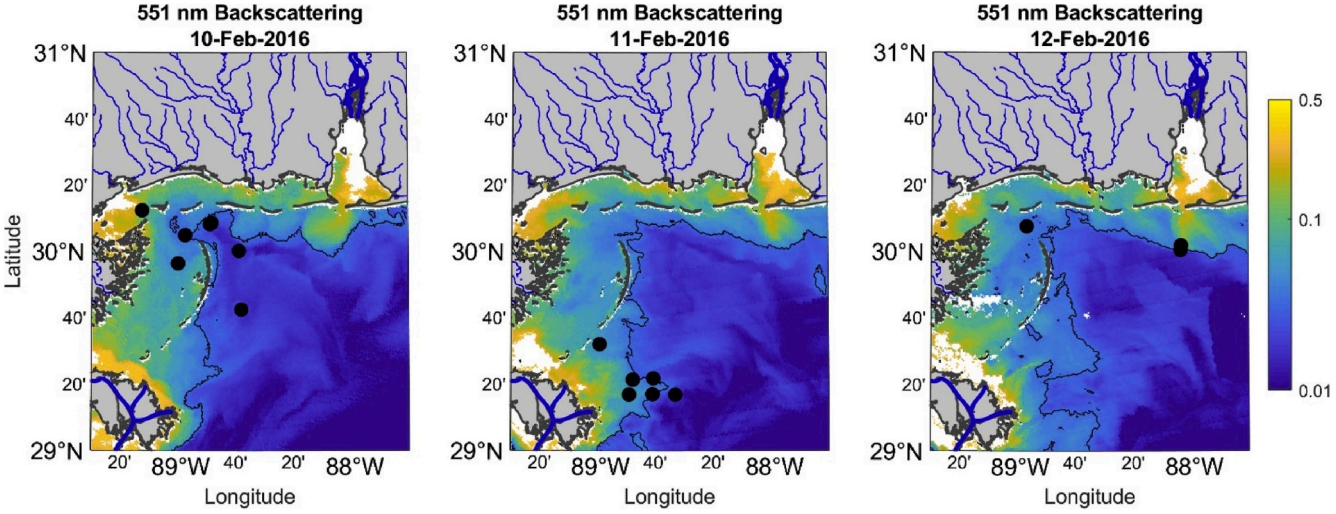

Fig. 5. Contours of optical backscattering at 551 nm (m^{-1}) at the surface, representing regions of freshwater plumes. Each subplot is a day of the cruise with the corresponding stations performed on that day as black dots. The black contour delineates the region of freshwater influence (using a value of 0.3 m^{-1}). Rivers are outlined in blue. (For interpretation of the references to color in this figure legend, the reader is referred to the Web version of this article.)

in comparison to the other eight years. Chl-a values were more than 2 mg m^{-3} higher than the 15-year monthly mean for most of the sounds and Mississippi Bight up to the 1000 m isobath. The largest (<3 mg m^{-3}) chl-a anomalies of 2016 were found in the northwest corner of the map (Lake Borgne Estuary) and south of the MSR Delta.

During the cruise, the extent of the freshwater plume showed some variability due to the complex dynamics of this coastal region (Fig. 5). Overall, freshwater plumes appeared to influence the Mississippi and Chandeleur Sounds the most. The Mobile Bay plume was transported westward on February 10, flowing into the western Mississippi Bight, and then eastward on February 11. Similarly, the MSR plume through the MSR Delta was confined near the coast on February 10 and expanded eastward on February 11 and 12. On February 11, a filament of high optical backscattering appeared to exit Lake Pontchartrain Estuary into the Chandeleur Sound, likely BCS waters. Freshwater entered the Mississippi Bight through various inlets between the barrier islands along the northern boundary and from south of the Chandeleur barrier islands with the eastward trajectory of the MSR plume. February 12 resulted in the largest extent of freshwater influence within the Mississippi Bight.

It is within this dynamic context that the stations were visited during the three-day cruise. In particular, note that station S3 located in the northwestern corner of the Mississippi Bight was visited on February 12 as the BCS waters spread eastward, while the nearby stations were sampled on February 10. Also note, the two stations outside Mobile Bay (MB1 and MB2 from Fig. 1) were taken on either side of a Mobile Bay plume front (Fig. 5).

3.3. Temperature and salinity distribution

The CTD casts taken throughout the western Mississippi Bight presented temperatures and salinities ranging from 11° to 23 °C, and 19 to 37 psμ, respectively (Fig. 6). The measurements at the Mooring Array (blue; see Fig. 1 for station locations) showed two distinct water masses: saltier warmer waters (higher density) below fresher cooler waters (lower density) consistent with the presence of a freshwater plume based on the optical backscattering on February 11 (Fig. 5). The Mooring Array salinities and temperatures were distinctly different from the areas closer to shore. The Inner Shelf (green), Chandeleur Sound (aqua), and Mobile Bay (red) stations had temperatures and salinities that overlapped each other across the TS diagram (except S1 and S2R within the Chandeleur Sound). These relatively shallow waters were colder but similarly salty relative to the surface layer at the Mooring Array. They were also fresher than the deeper waters at the Mooring Array but within a similar temperature range. The colder inshore waters resulted from heat loss during the passage of a cold front on February 8–9 (Fig. 7e). The freshest and coldest waters at S1 and S2R were from the shallowest areas, closest to the freshwater inputs within the Sound.

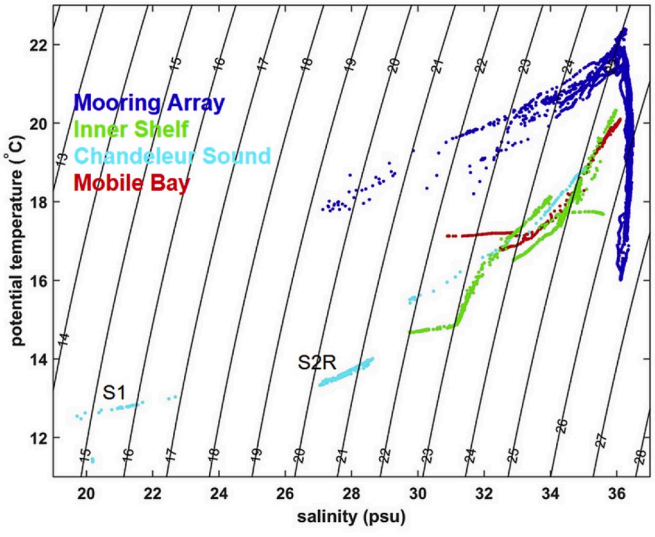

Fig. 6. Temperature-salinity diagram color coded with respect to different measurement areas (see Fig. 1): Mooring Array (blue), Inner Shelf (green), Chandeleur Sound (aqua), and Mobile Bay (red) areas. Black numbered contour lines represent density anomalies (kg m^{-3}). (For interpretation of the references to color in this figure legend, the reader is referred to the Web version of this article.)

3.4. Mooring array circulation

Mean currents near the MSR Delta (stations C1–C5 in Fig. 1b) between January 15 and February 15 were unidirectional, relatively weak (<0.3 m s^{-1}), and oriented to the north-northeast (toward the shelf) with surface currents nearly twice as strong as bottom currents and stronger surface currents at the shallower locations (C1 and C4) than the deeper sites (C3; Fig. 7a). The main variability (70% of the variance) of the currents during this period is represented by mode 1 (Fig. 7b). Mode 1 currents are unidirectional and oriented similar to the mean currents. These currents are modified by the amplitudes (Fig. 7d), where positive amplitudes reinforce the mean current patterns. Two days before the cruise a cold front generated relatively strong (~10 m s^{-1}) southeastward winds (Fig. 7e), lowering coastal water levels (setdown). The resulting coastal low surface pressure generated northeastward currents (>0.7 m s^{-1}) in response to the geostrophic balance between the pressure gradient and the Coriolis acceleration. This current transported the MSR plume toward the Mississippi Bight, as confirmed by optical backscattering on February 10–12 (Fig. 5). However, strong winds also result in vertical mixing of the surface layers.

Mode 2 represents the plume behavior (accounts for 8% of the total variance), showing a two layer, vertically-sheared flow with surface layer currents oriented nearly 180° out of phase from the bottom layer (Fig. 7c). Positive mode 2 amplitudes represent surface currents oriented toward the shelf similarly to the mean and mode 1. The strongest positive mode 2 amplitudes occurred during the cruise, when CTD casts indeed measured a stratified water column with fresher surface waters from the MSR (Fig. 6). Instances of zero mode 2 amplitudes appear to coincide with negative mode 1 amplitudes, when currents were oriented away from the shelf (e.g., January 15–22 and January 27-February 6) as a result of relatively weaker winds (~5 m s^{-1}) and transported well-mixed shelf waters.

3.5. Model results

The CONCORDE synthesis model allowed us to investigate the advection and transport of MSR-sourced BCS waters entering the Mississippi Bight from Lake Pontchartrain Estuary after January 10. Fig. 8d–f shows the modeled daily surface salinity fields with surface currents during the cruise period. BCS waters began flowing out of Lake Pontchartrain Estuary on January 16 and kept spreading eastward and southward through the research cruise days, as observed with the optical backscattering (Fig. 5). The MSR and Mobile Bay plumes also spread into the Mississippi Bight, northeastward and southward, respectively, most clearly depicted on January 30 (Fig. 8c) and February 11 (Fig. 8e). Model simulations showed an eastward expansion and dilution of freshwater from Lake Pontchartrain Estuary into the Chandeleur and Mississippi Sounds during the three-day cruise.

Model simulations tracked the movement of surface waters through neutrally buoyant simulated drifters, initiated in Lake Pontchartrain Estuary and Mobile Bay inlet (Fig. 9). Simulated drifters released at the start of the BCS opening on January 11 show that Lake Pontchartrain Estuary waters traveled into Mississippi Sound as well as into Chandeleur Sound hugging the western coast and entering Mississippi Bight after 30 days (Fig. 9c). At the same time, Mobile Bay waters traveled west mainly along the northern coast of Mississippi Bight and entered the Chandeleur Sound 15 days after the Spillway opening (Fig. 9g).

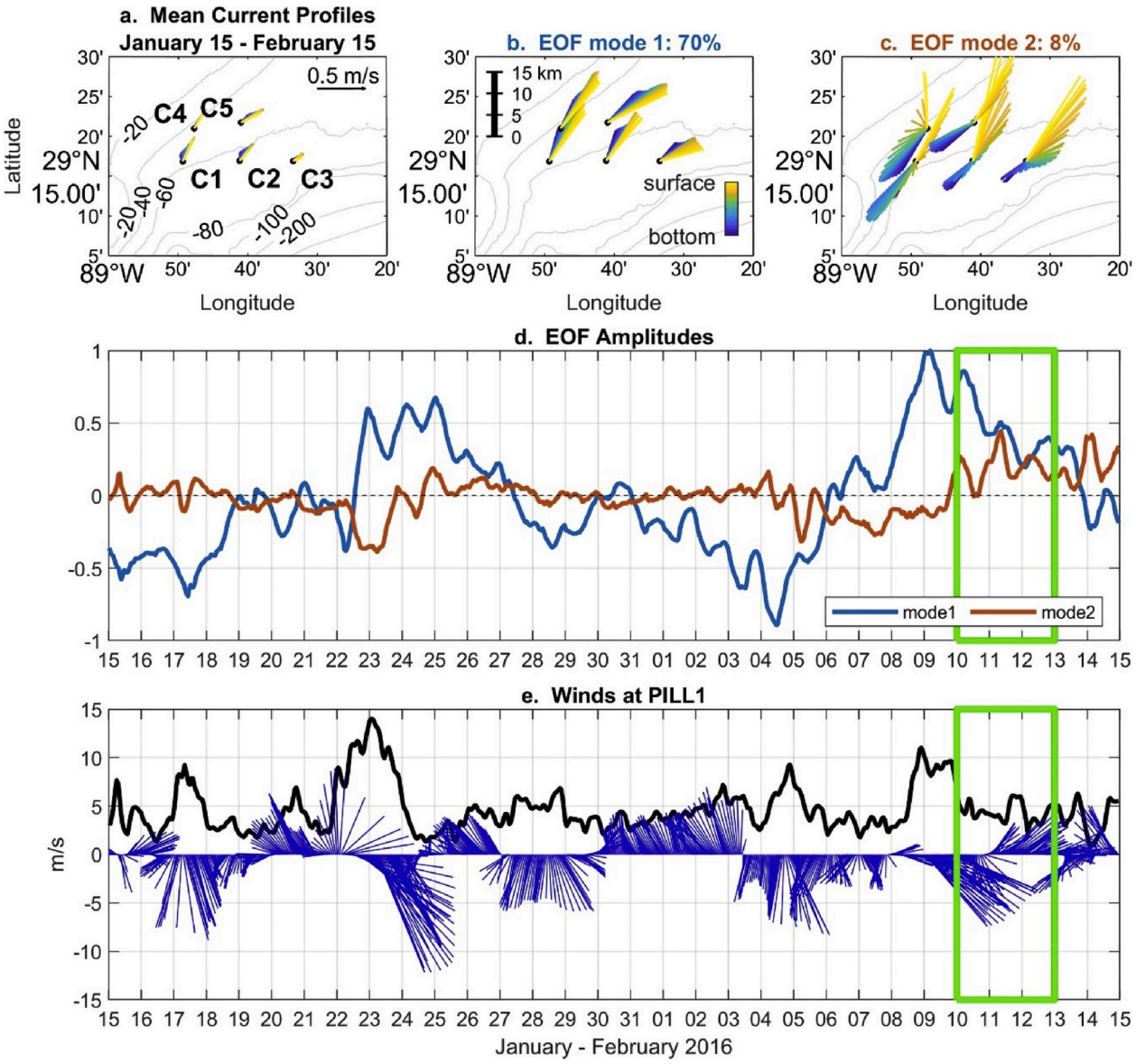

Fig. 7. Currents at the Mixing Array stations (C1–C5). (a) Mean current profiles from January 15 through February 15, 2016. Empirical orthogonal function (EOF) spatial patterns of modes (b) 1 and (c) 2 at all the moorings for the period January 15-February 15, 2016. (d) EOF temporal amplitude time series for modes 1 and 2. (e) Wind vectors (blue) and magnitude (black) in oceanographic convention (vectors pointed in the direction the wind is going) at the PILL1 station located on the MSR Delta (see Fig. 1 for location). Green box in (d) and (e) represents cruise period. The gray contours in (a)–(c) show the bathymetry as numbered in (a). (For interpretation of the references to color in this figure legend, the reader is referred to the Web version of this article.)

As simulated drifter release dates change, their trajectories also varied. Simulated drifters released from Lake Pontchartrain Estuary 10 days after the opening (January 21) traveled farther in Mississippi Sound towards Mobile Bay (Fig. 9d) while the simulated drifters released from Mobile Bay could not reach Chandeleur Sound (Fig. 9i). The eastward spread of Lake Pontchartrain Estuary simulated drifters was reduced after January 31 with every 10 day delay in simulated drifter release (Fig. 9e and f), as a result of a reduction of the BCS flow and subsequent decrease in sea surface height (SSH). Simulated drifters released from Mobile Bay increased their extent into Western Mississippi Sound, remaining closer to shore around the barrier islands while entering Mississippi Sound (Fig. 9i). Mobile Bay simulated drifters released on February 10 showed dramatically different paths due to shifting winds, largely remaining east of Mobile Bay and extending across the shelf (Fig. 9j).

Twin experiments were conducted based on two scenarios with and without the opening of the BCS discharge. The open BCS scenario resulted in an averaged SSH of 40 cm higher across the Lake Pontchartrain Estuary open boundary. Simulated drifters with the open BCS scenario managed to quickly exit Lake Borgne Estuary (driven by the higher SSH within Lake Pontchartrain Estuary), spread through Chandeleur Sound and enter the northwestern corner of the Mississippi Bight (Fig. 9c and d). The simulated drifters in the simulation with closed BCS remained within estuarine lakes Pontchartrain and Borgne, hardly entering the western Mississippi Sound.

3.6. *BCS water chemical signature and identification*

The MSR waters and local river sources had differing chemical signatures. MSR waters presented a much lighter $\delta^{18}O$ isotopic signature (−6.6‰) relative to AL/MS local rivers (−3.6‰). Ba concentrations were significantly higher for the MSR waters (443 nM) relative to local rivers (~220 nM; Table 2). The average concentration of Cs in MSR waters was estimated at 0.28 nM, while the AL/MS river waters

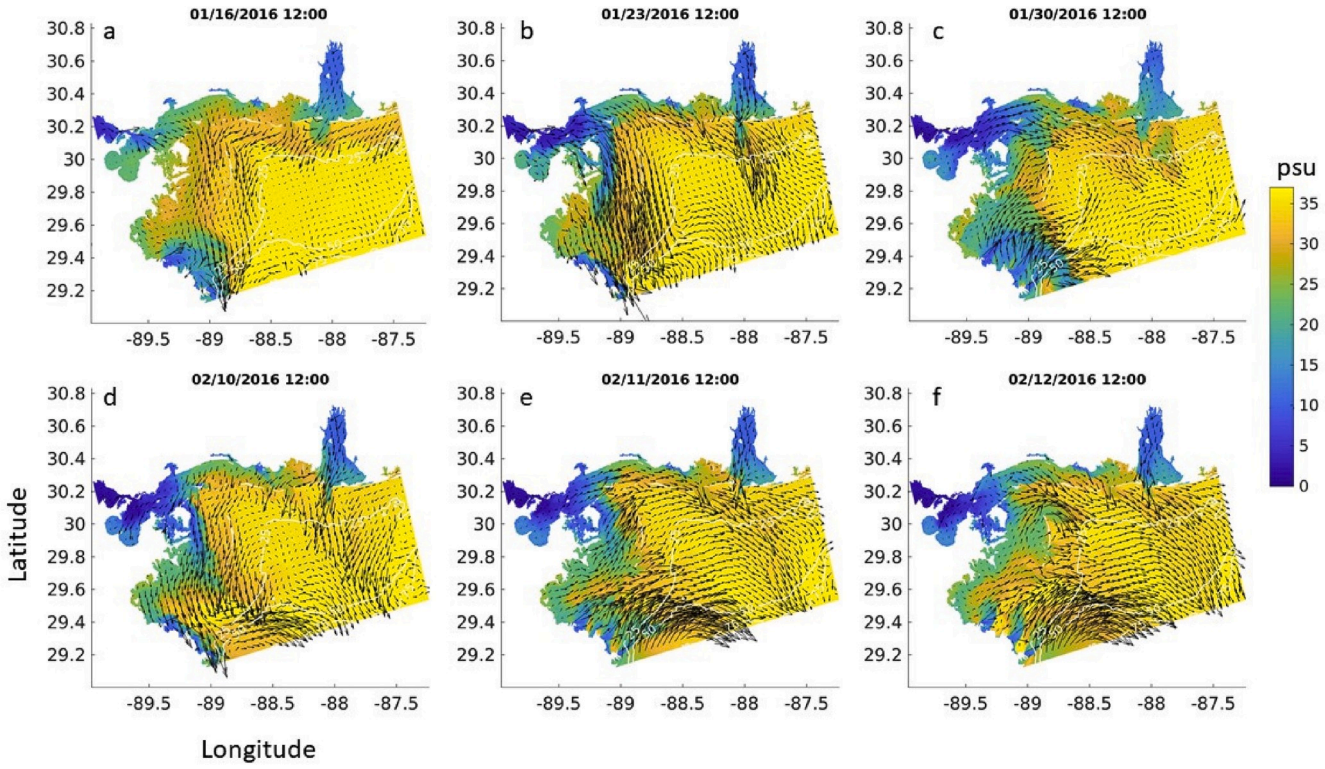

Fig. 8. Model results of surface salinity (psu) filled color contours with surface current vectors (black) after the opening of the Bonnet Carré Spillway (BCS) and during the cruise on (a) January 16 (6 days after BCS opening), (b) January 23, (c) January 30, (d) February 10 (cruise day #1), (e) February 11 (cruise day #2), (f) February 12 (cruise day #3). White contours are bathymetry every 25 m. (For interpretation of the references to color in this figure legend, the reader is referred to the Web version of this article.)

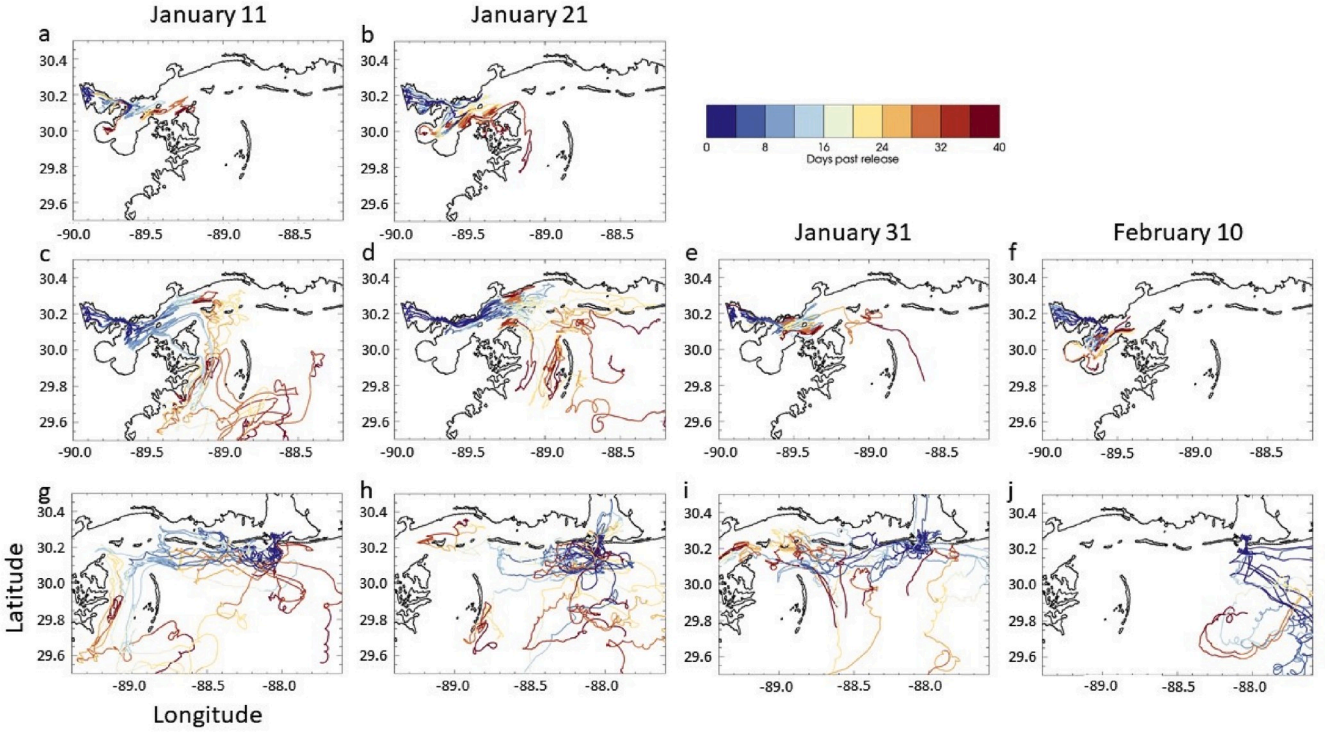

Fig. 9. The 40-day trajectories of simulated drifters simulated by the CONCORDE model. (a-b)Releases with a closed Bonnet Carré Spillway (BCS) from Lake Pontchartrain Estuary, (c–f) with an open BCS from Lake Pontchartrain Estuary and from the Mobile Bay main pass (g–j) on January 11th (a&c&g), January 21st (b&d&h), January 31st (e&i) and February 10th (f&j). The color tracks their duration with blue representing the release day and red as 40 days after the release. Black contour outlines the coast. (For interpretation of the references to color in this figure legend, the reader is referred to the Web version of this article.)

Table 2
Chemical compositions of freshwater discharging into the Mississippi Bight. Concentrations of dissolved inorganic nitrogen (DIN = NO_x + NH_4), phosphate, barium (Ba), Cesium (Cs), and oxygen isotope composition ($\delta^{18}O$) in the waters from the Mississippi and local rivers. Chemical compositions for the Mississippi River are also valid for the BCS discharge. The data correspond to the average concentrations and associated standard error of the five field trips conducted in each river between 2015 and 2016. The local rivers include the Pascagoula, Mobile, Pear, East Pearl, Jourdan, and Wolf rivers.

	DIN (μM)	PO_4 (μM)	$\delta^{18}O$ (‰)	Ba (nM)	Cs (nM)
Mississippi River	126 ± 13	2.3 ± 0.6	−6.6 ± 0.3	443 ± 42	0.28 ± 0.15
Local Rivers	12 ± 1.2	0.44 ± 0.08	−3.6 ± 0.2	235 ± 14	0.61 ± 0.11

contained 0.61 nM (Table 2). The DIN and phosphate concentrations in MSR waters (126 μM and 2.3 μM, respectively) largely exceeded those of the AL/MS local rivers (12 μM and 0.44 μM, respectively) (Table 2).

The MSR fraction estimated at each surface sample is shown in Fig. 10b and Fig. 11f. Shades of blue indicate a dominant contribution of local rivers while shades of red show a greater contribution of MSR waters. High contributions (>50%) of MSR waters were found at the Mooring Array stations (C1–C5 and BC) east of the MSR Delta (the usual path for MSR waters) with a decrease of MSR fractions away from the Delta. A relatively high MSR fraction (~30%) was also found at station S1 in the northwestern Sound, indicating the presence of the MSR waters from the BCS. MSR fractions were relatively low at stations S2 (0%) and S3 (~20%) in the Chandeleur Sound despite the low salinity, suggesting the presence of freshwater originating from the AL/MS local rivers.

The salinity and associated MSR water fractions explain the variations of Ba, Cs, and nutrients (Fig. 11e–h). Regarding the Mooring Array stations, the MSR fractions suggest MSR waters as the main contributor to stations BC, C1, and C4. This is in agreement with low Cs and high Ba concentrations measured at these stations (Fig. 11g and h). On the other hand, stations C2, C3, and C5 had higher salinity but still relatively high MSR fractions, with lower Ba and higher Cs concentrations. The high DIN and phosphate concentrations, relative to the other stations influenced by AL/MS local rivers indicate the presence of MSR at these stations (Fig. 11i and j). These stations (C2, C3, C5) were also highly influenced by local river waters (between 50 and 60%) even though they are very close to C1 and C4, highlighting the large spatial variability in freshwater sources.

3.7. Optical water mass classification

The underway optical data characterized the different water masses in terms of optical constituents such as chl-a, CDOM and sediments. MSR waters were generally CDOM-dominated (light and dark blue in Fig. 10c). Waters along the northern cruise track (spanning from east to west nearest Mobile Bay and Mississippi Sound) where chl-a dominated with higher scattering (red to green). The areas near the MSR Delta were characterized by CDOM-dominated waters (blue), with higher scattering near the Delta and lower scattering offshore. Scattering was high (>2.5 m^{-1}) near the coastal areas and river regions, especially near the outflow of Mobile Bay and within Chandeleur Sound. Scattering was lower farther offshore (blue).

The backscattering at 685 nm along the northern cruise transect

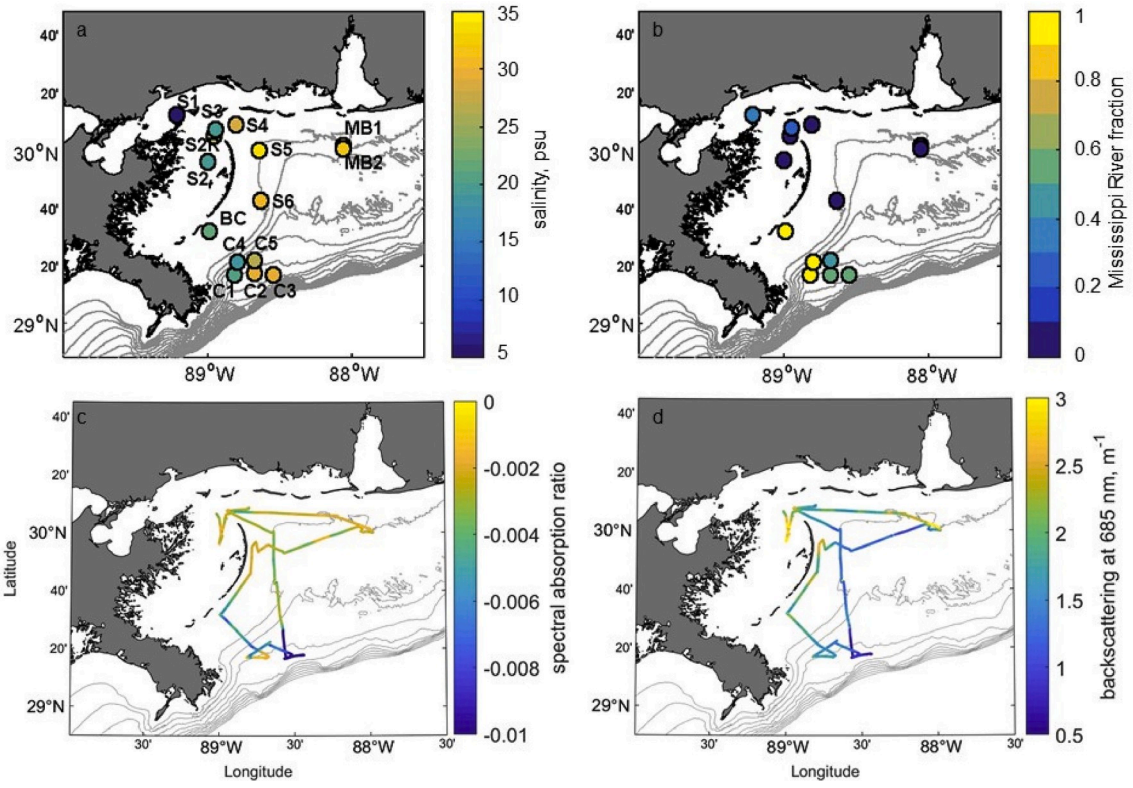

Fig. 10. Distribution of the origin of freshwater in the Mississippi Bight. (a) Surface salinity values, and (b) fraction of Mississippi river waters estimated at each station (Sanial et al., 2019). (c) Surface spectral absorption ratio and (d) scattering at 685 nm (m^{-1}) along the cruise track. Note that the Mississippi River fraction was not estimated at station S5 because of the low freshwater influence based on the high salinity at this station. The gray contours show the bathymetry every 10 m from 20 m to 200 m.

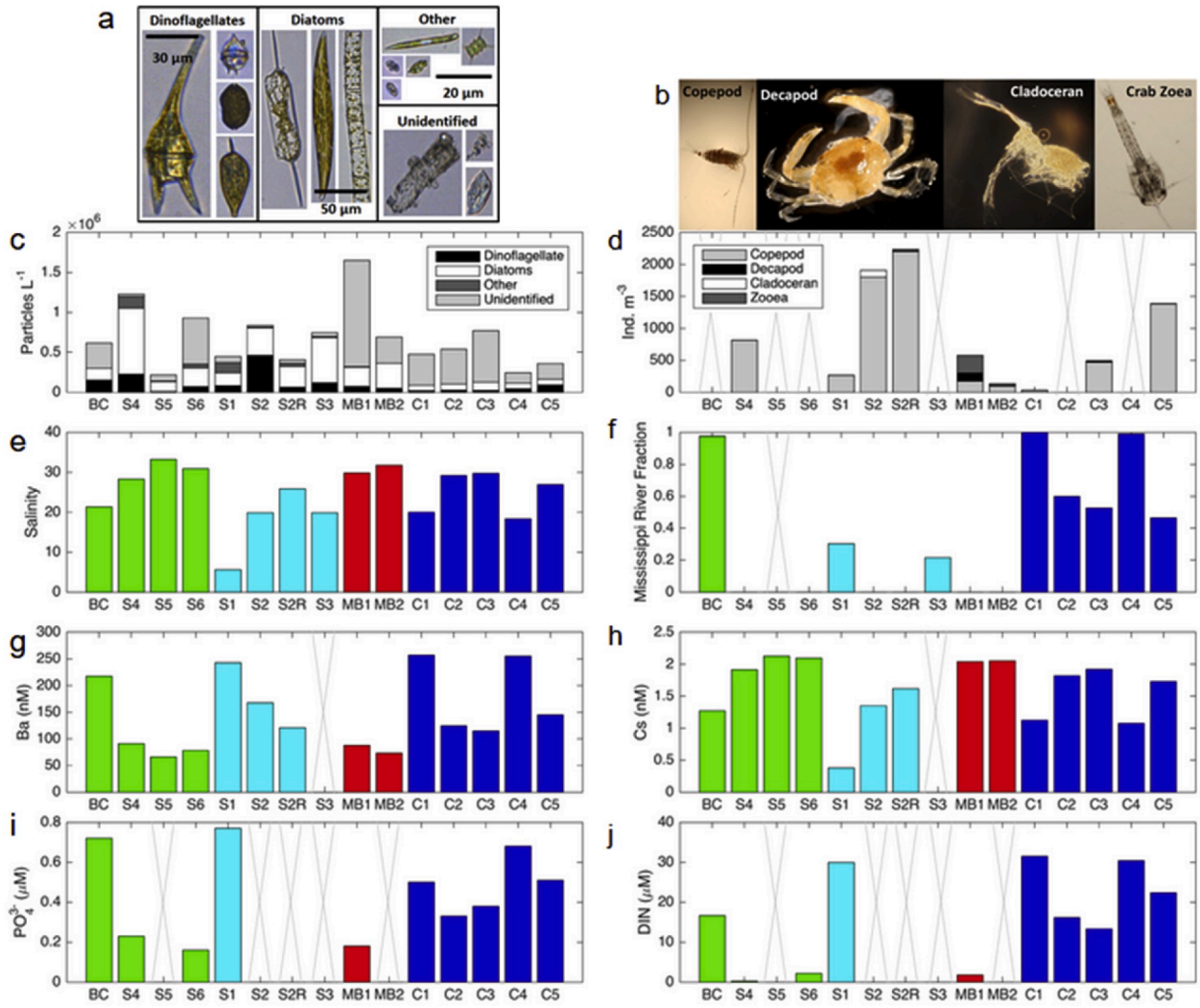

Fig. 11. Pictures (a,b) and concentrations of biological and chemical parameters at each station: (c) microplankton and zooplankton broken down into different categories, (e) salinity, (f) Mississippi River Fraction, (g) barium (Ba), (h) cesium (Cs), (i) phosphate (PO_4^{3-}), and (j) dissolved inorganic nitrogen (DIN). The color code is based on the station locations (cf Fig. 1. Mooring Array: C1–C5; Mobile Bay: MB1, MB2; Chandeleur Sound: S1–S3, S2R; Inner Shelf: BC, S4–S6). (For interpretation of the references to color in this figure legend, the reader is referred to the Web version of this article.)

parallel to the barrier islands (Fig. 10d) alternated between higher (orange/yellow) and lower (green) concentrations, which represents higher scattering Mississippi Sound waters exiting between barrier islands into lower scattering waters on the shelf. The gradients in spectral absorption ratio and backscattering at 685 nm (Fig. 10a and b), observed away from the MSR Delta and across the Mooring Array, were consistent with the decrease in MSR fraction away from the Delta and concentrations of Ba, Cs, and nutrients (Fig. 11) as well as with the optical backscattering maps (Fig. 5).

3.8. *Phytoplankton and zooplankton spatial patterns*

Dinoflagellates and diatoms were the dominant microplankton taxa during the cruise, constituting 17.4 and 40.6% of total plankton abundances, respectively (Fig. 11a,c). Unidentified particles comprised a majority of the total imaged biomass at most stations (37.9% on average), particularly at MB1 (located within the Mobile Bay plume) where they comprised 85.2% of the total particles. Station S4 had the highest particle concentrations (excluding unidentified particles), with dinoflagellates (2.3×10^5 particles L^{-1}) and diatoms (8.5×10^6 particles L^{-1}) contributing nearly 12 and 45% of the total classified images, respectively. Similar proportions of dinoflagellates and diatoms were found at S3. Nearly half of the particles at S2 were diatoms and the other half dinoflagellates. Stations C1–C5 generally had lower particle concentrations, ranging from 1.1×10^5 to 2.4×10^5 particles L^{-1} (Fig. 11a).

Total zooplankton concentrations varied significantly among different regions (Kruskal-Wallis test, $H = 8.88$, $df = 2$, $p = 0.012$), with the highest concentration in the Chandeleur Sound relative to the Birdfoot Delta and Mobile Bay ($p < 0.01$) (Fig. 11b,d). Copepods (calanoids + cyclopoids) were by far the most dominant of all zooplankton groups, and their concentrations also varied significantly among different regions (Kruskal-Wallis test, $H = 9.43$, $df = 2$, $p = 0.009$), with the highest concentration in the Chandeleur Sound (S2 and S2R; $p < 0.05$; Fig. 11d).

Cluster analysis using SIMPROF identified spatial structure in the composition of phytoplankton and microzooplankton, as well as zooplankton communities within the study area (Fig. 12a and b). For phytoplankton and microplankton community composition, two significant clusters were identified (ANOSIM: $R^2 = 0.76$, $p = 0.001$): one corresponding to all of the stations near the Birdfoot Delta (Cluster I of BC and C stations), and the other corresponding to stations near the barrier islands (S stations; Cluster I) and near Mobile Bay (MB1 within the plume and MB2 just outside the plume; Fig. 12a). SIMPER analysis revealed that "other" (i.e., nanoflagellates and chlorophytes)

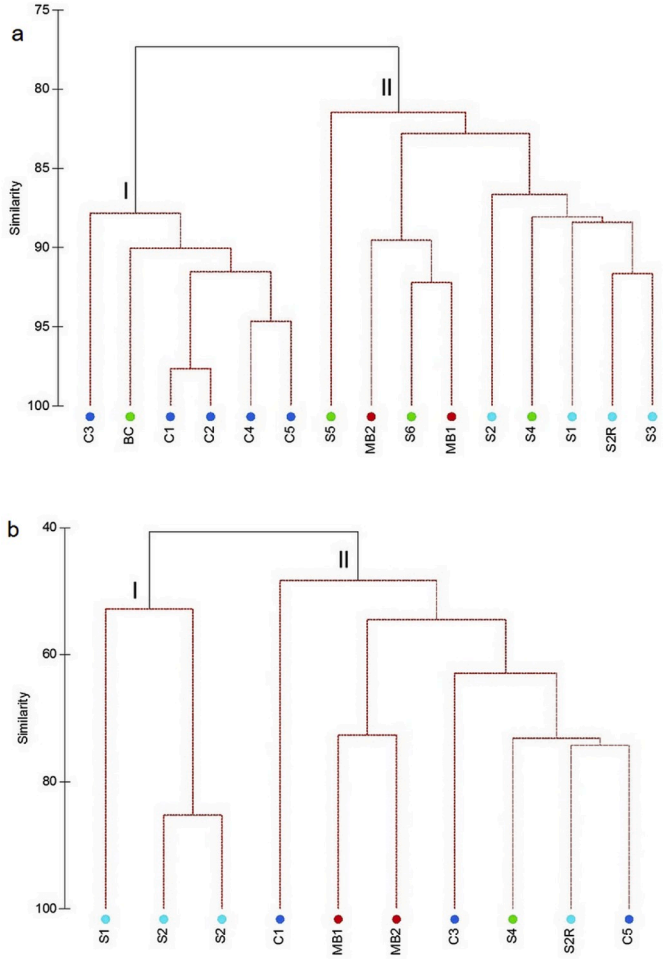

Fig. 12. Two cluster analyses. (a) Cluster analysis of microplankton – Two main clusters (I and II) corresponding to MSR influence and Mobile Bay and other River influence. The MSR water detected at S1 was not sufficient to change the microplankton community into one that resembles C1–C5 and BC stations. (b) Cluster analysis of zooplankton community composition by station showing two (I & II) main clusters. S1 and S2 stations are different from other stations.

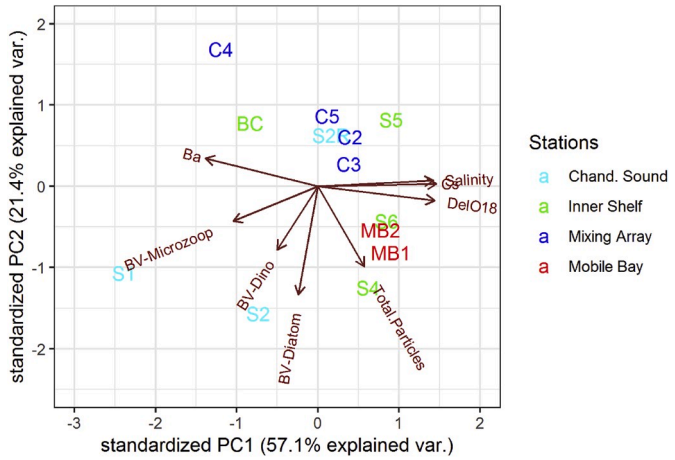

Fig. 13. PCA combining the biological (microplankton only, biovolumes and total particle count) and chemical data at the stations. Any station with missing data has been removed. PC1 contains most of the physical and chemical data, while PC2 has mostly the biological data. Phytoplankton biovolumes (BV) are positively correlated with one another and with chl-a. S1 and S4 generally had high abundances of microzooplankton and phytoplankton (total particles), respectively. Stations S6 and MB1 had relatively high salinity, Cs, and $\delta^{18}O$, as well as total particles.

contributed most (37%) to the total dissimilarity between clusters, followed by the concentration of particles (24%), diatoms (19%) and dinoflagellates (14%).

For the zooplankton community, cluster analysis with SIMPROF also grouped all samples into two distinct clusters (ANOSIM: $R^2 = 0.67$, $p = 0.008$): Cluster I consisted of stations from the Chandeleur Sound region (except S2R), while Cluster II was composed of the remaining stations (Fig. 12b). SIMPER analysis revealed that copepods contributed most to the total dissimilarity in community composition between clusters (23%), followed by cladocerans (17%), other decapods (10%), chaetognaths (9%), barnacle nauplii (7%), larvaceans (6%), zoea larvae (5%), siphonophores (5%), ostracods (4%), copepod nauplii (3%). The rest of the zooplankton taxa (nine taxa) combined contributed 10% to the total dissimilarity between clusters.

Spatial relationships among microplankton and chemical variables were examined with a PCA analysis for stations with a complete set of measurements, all stations except S3 and C1 (Fig. 13). Ba acted as a proxy for DIN and phosphate because they were highly correlated ($r = 0.90$ and 0.97, respectively). Chl-a was also correlated with phytoplankton biovolume ($r = 0.73$), so chl-a was dropped from the analysis. Principal component 1 explained 57.1% of the variability, with the largest loadings for Cs, $\delta^{18}O$, and salinity, while principal component 2 contained a larger proportion of the biological data (21.4% of the variability). The largest loadings were for diatom and dinoflagellate biovolumes, as well as total particles. Stations S1 (station within the Chandeleur Sound with the lowest salinity and a significant percentage of MSR water, Fig. 11) and S4 (with no traces of MSR waters) had high abundances of microzooplankton and phytoplankton (total particles), respectively. The BC and C stations closer to the MSR Delta had relatively high nutrient content (correlated with high levels of Ba) but lower phytoplankton and microzooplankton biovolumes compared to the more nearshore stations within the Mississippi and Chandeleur Sounds and outside Mobile Bay.

4. Discussion

This study combined field sampling, modeling, and remote sensing to characterize the oceanographic conditions and biogeochemical response within a broad coastal region shortly after the opening of the BCS in 2016. For the primary sources of freshwater (MSR and local river watersheds) to the Mississippi Bight, which is located within the northern Gulf of Mexico, total discharge was anomalously high during winter and resulted in an unprecedented early opening of the BCS. These large freshwater pulses can generate higher than average biological production, similar to El Niño effects observed in this region during winter and spring (Gomez et al. 2019). The BCS represents an intermittent and infrequent pathway for MSR waters into the Mississippi Sound, Chandeleur Sound, and Mississippi Bight. This region is usually dominated by freshwater from smaller local rivers and the Mobile Bay watershed, with only seasonal influence from the MSR (Morey et al. 2003; Dzwonkowski et al. 2018b; Ho et al. 2019; Sanial et al. 2019). Measurements and model results generally agreed that BCS waters were confined to the northwestern portion of the study area before and during the field sampling. While numerous studies have examined the immediate response of the ecosystem to freshwater plumes in this region (Bargu et al. 2011 and some others cited later), few examined the broader scale response to a BCS opening, particularly a release under relatively low stratification that is more common during the winter months. We highlight the main drivers of the movement of BCS waters, the associated biogeochemical and ecological patterns found during this release, and how these conditions compared to other BCS openings.

4.1. The 2016 BCS opening

4.1.1. Time scale of the plume into the Mississippi Bight

Model results, along with water chemistry and optical backscattering, suggested that the BCS waters slowly (within 4–5 weeks) migrated out of Lake Pontchartrain Estuary and mostly remained within the Mississippi and Chandeleur Sounds. The BCS waters were driven out of Lake Pontchartrain Estuary by a SSH increase within the lake created by the temporary discharge of the BCS. However, the slow speed of the BCS waters out of Lake Pontchartrain Estuary and Lake Borgne Estuary allowed the winter wind patterns to mix and dilute BCS waters with ambient waters and worked to confine BCS waters within the sounds. Thus, the transport and spread of BCS waters onto the shelf was limited. Samples of the BCS waters within the Mississippi and Chandeleur Sounds were patchy as shown by in situ chemistry data and strong temporal variability exemplifies the difficulty in evaluating the influence of the BCS opening based on limited coverage of in situ data. As an example, stations S4 (sampled on 02/10, 15:19) and S2R (02/10, 12:55) showed no MSR (from the BCS) contributions although they had relatively low salinities, especially at S2R (Fig. 11f). Just two days later, nearby station S3 (02/12 20:03) showed a significant MSR (from the BCS) contribution.

4.1.2. Dilution with local waters and effects from wind and SSH

Currents at the Mooring Array along with model results showed that winds were the primary driver of circulation, especially with the passage of cold fronts. Wind has been previously identified as a major driver of the mixing and fate of the MSR plume in coastal areas (Walker 1996; Morey et al. 2003; Walker et al 2005; Schiller et al. 2011; Dzwonkowski et al. 2018a). The frequent fall and winter cold fronts (every 3–10 days) generate relatively strong southward winds (>10 m s^{-1}) that push the plume toward the west and south, and mix shelf waters. On the other hand, spring and summer consist of weaker (<5 m s^{-1}) northward winds that transport the MSR plume eastward into the Mississippi Bight (Schiller et al. 2011; Dzwonkowski et al. 2018a). With this wind seasonality and subsequent MSR transport, BCS waters would take starkly different paths depending on the time of year. The results from the 2016 BCS opening presented here show that the BCS plume largely remained within the estuarine lakes and the sounds. Conversely, we would expect that spring and summer mild northward winds would most likely result in BCS waters traveling eastward into the Mississippi Bight.

The MSR discharge flowing out of the Birdfoot Delta was much larger than the waters diverted via the BCS (less than 10% of MSR waters). MSR fraction analysis results indicated that the MSR had a larger presence on the shelf near the Delta (from the MSR normal outflow) than within the Mississippi Sound and Chandeleur Sound (from the BCS). Nevertheless, both MSR waters at the Mooring Array stations (from the Birdfoot Delta) and at the entrance of Lake Borgne Estuary (from the BCS) were quickly diluted with local freshwater sources, as observed by the gradient in MSR fraction. While individual local river discharge is relatively small, collectively these rivers are equivalent to up to 40% of the MSR discharge that travels east and offshore (Dzwonkowski et al. 2018b). Our results show that MSR transport was localized, while smaller rivers were the dominant source of freshwater in the Bight, as a result of the local river flooding from December and into January.

4.1.3. Plankton community composition

One of the motivating factors for this study was to determine whether the opening of the BCS would potentially influence the phytoplankton community, perhaps even triggering a harmful algal bloom. Indeed, larger nutrient concentrations could potentially result in algal blooms (Turner et al. 2004), but this was not observed in our case. Model simulations and water mass tracer data show that Mobile Bay and local river waters seemed to play a much greater role structuring plankton communities along the inner shelf, whereas the MSR from the Birdfoot Delta played a much greater role in the outer shelf. The different water sources consisted of different nutrient ratios. Redfield ratio shows that the N:P ratio was <16 at stations along the outer shelf, suggesting N-limitation (Redfield 1958; Hillebrand and Sommer 1999), but the N:P ratio was much greater than 16:1 at stations along the inner shelf, suggesting that P was a limiting nutrient.

Phytoplankton biomass and community structure in the Mississippi Bight are influenced by the proximity, magnitude, and timing of the nutrient-rich fluvial input into the system (Qian et al. 2003). Although research on this coupling is limited, several studies point to a nearshore succession of plankton groups in response to nutrient inputs. Phytoplankton succession in Lake Pontchartrain Estuary in years of spillway openings during the warmer spring and summer months show elevated diatom concentrations were followed by late summer cyanobacteria blooms (Bargu et al. 2011; Roy et al. 2016). Previous studies in the region have shown that diatoms are one of the most common phytoplankton in the Mississippi Bight (Qian et al. 2003; Chakraborty and Lohrenz 2015). Cyanobacteria often peak in abundance along the inner shelf and in estuaries during summer, when warmer temperatures, weaker winds and reduced discharge conditions increase residence times (Paerl 1996; Li 1998; Chakraborty and Lohrenz 2015). Cyanobacteria blooms were extensive during the second BCS opening in 2019 that spanned from mid-May through the end July. The resulting nutrient pulse generated dense toxic phytoplankton populations that closed many beaches spanning from Lake Pontchartrain Estuary through the Mississippi coast and affected many marine animals including dolphins, oysters, and coastal fisheries (e.g., Chappell, 2019).

Conditions during the wintertime 2016 BCS opening were not favorable for a bloom (cold mixed water column); however, BCs openings later in the season could be more likely to trigger an algae bloom. Haywood et al. (2018) found that carbon-cycling processes were suppressed within Lake Pontchartrain Estuary following the 2016 BCS opening. This suppression was correlated to a sharp decrease in water temperatures within the estuary from ~11 °C before the opening to ~5 °C during the opening. Lower water temperatures have been linked to limited carbon-cycling processes (Arnosti and Jørgensen, 2003; Hernes et al., 2008; Weston and Joye, 2005).

The zooplankton community composition varied spatially, with most samples from the same regions containing similar communities. The dissimilarity in zooplankton composition among regions was primarily driven by changes in relative abundance of calanoid copepods, which were significantly more abundant in the Chandeleur Sound relative to other stations, and were the most abundant zooplankton taxa in all the stations. In this region, these small crustaceans are common and are an important prey item for many species of fish (Baier and Purcell 1997), including commercially important ones such as the Gulf Menhaden (Govoni et al. 1983). Environmentally induced changes in their abundance could affect fish growth, reproduction, and survival.

4.2. Comparing 2016 to other openings

Table 1 shows the average BCS discharge of MSR waters was approximately 14.7 km^3 while the highest discharge of 30.1 km^3 goes back to 1945. The effects of these discharges on the Mississippi Bight stratification can be considered by estimating its effect on the surface layer defined as a 5 m deep surface layer across the entire surface of the Mississippi Bight (approximately 48 km^3, 95 km × 100 km x 5 m). Assuming that all BCS waters entered the Mississippi Bight and that freshwater remained at the surface, the input of 2016 BCS waters would represent 15% of the volume of the Mississippi Bight surface layer, 29% based on the average BCS discharge, and up to 63% based on the maximum total discharge from the 1945 opening. This contribution of 15% of BCS water into the Mississippi Bight surface layer would result in a salinity drop of 5 psμ (assuming a background salinity for the surface layer of 36), 10 psμ for the average discharge, and up to 23 psμ for the largest total discharge observed. For the 2016 BCS opening, the average salinities for model results from the twin experiments over areas

shallower than 30 m (~47 km^3) showed a salinity difference of ~3 psμ. These values (~5 psμ bulk estimate vs ~3 psμ for model) are of the same magnitude, although differences could be attributed to freshwater likely extending below 5 m in the model especially in the sounds and Mississippi Bight. These estimates show that BCS openings have widespread effects across the Mississippi Bight.

Intrusion of MSR waters through the BCS would also affect the nutrients available for phytoplankton production. Nutrient (DIN) fluxes were estimated and compared for both BCS waters and local rivers. For the 2016 BCS opening of 6.9 km^3, a DIN concentration of 126 μM (Table 2) represents a flux of 8.69×10^8 mol (12,200 Mg) into the sounds and Mississippi Bight. In comparison, the total volume of water from the local AL/MS rivers over the 23 days of BCS opening from January 10 to February 1, 2016 (based on data from USGS: https://waterdata.usgs.gov/nwis) was estimated at approximately 8.8 km^3, around 20% more than the total BCS discharge. Considering a local river DIN concentration of 12 μM (Table 2), the AL/MS local rivers represented a DIN flux of 1.06×10^8 mol (1480 Mg) to the Mississippi Bight. Therefore, the DIN flux from BCS waters were one order of magnitude larger than local rivers. The DIN flux for the 2016 opening is comparable to other BCS openings (Roy et al. 2013).

The intermittent increase in nutrients and resulting primary-production from BCS openings could also exacerbate the summertime hypoxia commonly observed in the Mississippi Bight. Increased MSR discharges enhance primary production and plankton concentrations in the Mississippi Bight because of the larger nutrient fluxes and increased stratification. These factors usually contribute to a spreading of the bottom hypoxic layer along the shelf from Texas through Florida (Brunner et al. 2006; Bianchi et al. 2010; Dzwonkowski et al. 2018a; Ho et al. 2019). The Spillway opening in 2011 may have increased hypoxia in the northwestern Mississippi Bight (Ho et al. 2019). The wintertime 2016 BCS opening did not result in reported hypoxia on the shelf, likely because of the winter cold fronts known for mixing the shelf water column (Bianchi et al. 2010). Hypoxia in the Mississippi Bight is most common in late spring and summer, when shelf stratification increases because winds are greatly reduced. Therefore, a BCS opening during these warmer months could exacerbate hypoxia in the Mississippi Bight. Comparable to strong winter winds are intermittent tropical cyclone winds in summer and fall months. Tropical cyclones have been found to eradicate existing hypoxia in the northern Gulf of Mexico shelf by mixing the summertime stratification and hypoxic bottom layer: Hurricane Andrew in 1992 (DiMarco et al 1995, 2001), and Hurricane Cindy and Hurricane Dennis in 2005 (Rabalais et al. 2007).

BCS openings occur during uncharacteristically wet periods across the MSR watershed. Large-scale precipitation patterns across the US are influenced by climate variability such as El Niño Southern Oscillation (Enfield, 2001; Clark et al. 2014), where positive El Niño events result in increased precipitation across the MSR watershed and, thus, increased MSR discharges into the Mississippi Bight (Sanchez-Rubio et al. 2011; Gomez et al. 2019). El Niño events do not always coincide with BCS openings, although openings in 1973, 1983, 1997, and 2016 occurred either during or after an El Niño event. The BCS openings in 1983, 1997, and 2016 occurred during some of the strongest El Niño event in the last 70 years (Cohen et al. 2017). These years clearly resulted in greater precipitation over the MSR watershed, especially in the 2015–2016 winter that resulted in the warmest and wettest December on record (NOAA 2016). These connections highlight the effects from El Niño events on increasing MSR discharges that ultimately result in intermittent physical and biogeochemical changes in the Mississippi Bight.

4.3. Lessons learned

4.3.1. Key factors in evaluating the regional impact of BCS openings

The extent and spread of the BCS plume through the estuarine lakes and sounds depends on total discharge volumes, seasonal wind patterns, and stratification of the region. The 2016 BCS plume remained within the estuarine lake system and sounds, driven by both a short BCS duration and relatively strong north-northeasterly winds. Therefore, different seasons would affect the BCS plume trajectory in different ways. The generally weaker southerly winds of late spring and early summer would allow the plume to spread further out into the sounds and shelf. Furthermore, stratification during these periods would be enhanced. A larger extent of the BCS waters could affect the production of blooms, enhance the summer hypoxic layer in the Bight, and have a larger effect on the ecosystem.

4.3.2. BCS discharge effect on coastal ecosystem

The BCS openings have spanned from January through July since its construction in 1931 (Fig. 2), so the ecological effects on the coastal ecosystem have a seasonal component. This study assessing the mixing and transport of BCS waters (processes on small spatiotemporal scales), along with the associated biology, was conducted after the earliest opening of the spillway in January–February 2016, which represent conditions that are atypical for BCS openings, as 50% of them have occurred in spring, between April and May. Increasing the diversion of MSR through the BCS, especially in summer when the water column is already stratified, likely increases the development of hypoxia in the Mississippi Bight, disrupting oyster farming (Day et al. 2009; Roy et al. 2016; Posadas BC and Posadas BKA 2017) and fishery production (Lohrenz et al. 1997; Grimes 2001) in the region.

Furthermore, increasing global temperatures and extreme weather are expected to increase the potential for earlier openings such as this 2016 event. Global warming is expected to bring wetter winters to the eastern US and Great Plains (Karmalkar and Bradley 2017). Specific to the Midwest, climate model predictions by Wuebbles and Hayhoe (2004) suggest increases in winter and spring precipitation and temperature through 2099. Heavy precipitation events in the Midwest have already shown significant increases over the past century (Kunkel 2003; Angel and Huff 1997). Warmer temperatures in winter and spring will also lead to less snow accumulation with greater rainfall and flooding in the upper MSR watershed (Wuebbles and Hayhoe 2004).

5. Conclusions

The 2016 BCS opening was the earliest on record and third smallest, resulting from a strong El Niño that created the warmest and wettest December on record in the continental US. The wintertime opening of the BCS appeared to reduce its spread out of Lake Pontchartrain Estuary, as it was suppressed by the circulation impacted by the wind and short BCS opening duration. Furthermore, the concurrent flooding of the smaller local rivers further diluted the effects of the nutrient-rich BCS waters in estuarine lakes and sounds.

As this work demonstrates, the physical conditions surrounding the BCS opening are critical for determining where the fresh, high nutrient waters will be advected. Although the ecological impacts of this particular 2016 opening appeared to be minimal, the record long second opening of 2019 resulted in a number of acute and conspicuously negative ecosystem impacts. These impacts included extremely low salinities in the Mississippi Bight (5 psμ, Dzwonkowski personal communication); widespread cyanobacteria blooms (Mississippi Department of Environmental Quality); dolphin die offs (McConnaughey 2019); high mortality rates in oyster farms (Newton 2019); and low fishery yields (Lee 2019). In contrast, our study showed general confinement of BCS waters to the Chandeleur Sound, which may have reduced its overall ecological impacts because these areas consistently have low salinities. An approach similar to the one used in this study, combining modeling, remote sensing, and in situ physical and biogeochemical data, could be replicated in different seasons of BCS openings to elucidate the most important factors contributing to their deleterious ecological consequences.

Declaration of competing interest

The authors declare that they have no known competing financial interests or personal relationships that could have appeared to influence the work reported in this paper.

Acknowledgements

The authors would like to thank the CONCORDE and GOMRI community without whom this study would not have been possible. The cruise was very successful thanks to Captain Nic Allen and the entire crew of the R/V Point Sur. We acknowledge the hard work and contributions from the research cruise personnel: Adam Boyette, Alan Wiedemann, Wesley Goode, Alison Deary, Hannah Box, Sergio Derada, Sabrina Parra, Peng Ho, Laura Whitmore, Kelia Axler, Anne Griffis, Allison Mojzis, and Andrew Quaid. The following consortia participated in the cruise: CONsortium for oil spill exposure pathways in COastal River-Dominated Ecosystems (CONCORDE), Ecosystem Impacts of Oil & Gas Inputs to the Gulf (ECOGIG), Deep-Pelagic Nekton Dynamics of the Gulf of Mexico (DEEPEND), Alabama Center for Ecological Resilience (ACER), and Consortium for Advanced Research on Transport of Hydrocarbons in the Environment (CARTHE). Special acknowledgements to the Department of Marine Science (DMS) and the Gulf Coast Research Laboratory (GCRL) at The University of Southern Mississippi (USM), Louisiana Universities Marine Consortium (LUMCON), University of Georgia (UGA), and the Naval Research Laboratory (NRL) for providing personnel and equipment. Also special recognitions to Alan Shiller, Jerry Wiggert, Jeff Book, Frank Hernandez, Stephan Howden, and Bob Arnone for your thoughtful advice and guidance in this process.

We appreciate the US Army Corps of Engineers for making BCS discharge data publicly available, and Erick M. Swenson for organizing the BCS discharge time series for all the openings. This research was made possible by a grant from the Gulf of Mexico Research Initiative, United States. All data are publicly available through the Gulf of Mexico Research Initiative Information & Data Cooperative (GRIIDC) at https://data.gulfresearchinitiative.org. Doi numbers for the presented data are as follows: 10.7266/N79C6VGW for ADCP, 10.5067/AQUA/MODIS/L3M/CHL/2014 for remote sensing, 10.7266/N7416V4D for VIIRS backscattering, 10.5067/GPM/IMERG/3B-MONTH/05 for accumulated precipitation from NASA's Integrated Multi-satellite Retrievals for Global Precipitation Measurement, 10.7266/n7-w5y1-bc57 for microplankton, 10.7266/N73B5XKG for CTD casts, 10.7266/N70000H4 for bio-optics and flow-through, 10.7266/N7P55M4G for CONCORDE Synthesis Model output, 10.7266/N72F7KHX for CMA atmospheric forcing, 10.7266/N7542KZP for NCOM model output, 10.7266/N75T3J3B for biogeochemistry and trace metals, 10.7266/n7-sps7-rq23 for river discharges, and 10.7266/n7-5faw-an77 for zooplankton.

References

Grimes, C.B., 2001. Fishery production and the Mississippi river discharge. Fisheries 26 (8), 17–26. https://doi.org/10.1577/1548-8446(2001)026<0017:FPATMR>2.0.CO;2.

Adebayo, S., Amer, R., 2017. Impacts of the Mississippi River spillway opening on faecal coliform concentration in Lake Pontchartrain. River Res. Appl. 33, 1327–1335. https://doi.org/10.1002/rra.3179.

Álvarez, E., Moyano, M., López-Urrutia, A., Nogueira, E., Scharek, R., 2014. Routine determination of plankton community composition and size structure: a comparison between FlowCAM and light microscopy. J. Plankton Res. 36 (1), 170–184. https://doi.org/10.1093/plankt/fbt069.

Angel, J.R., Huff, F.A., 1997. Changes in heavy rainfall in Midwestern United States. J. Water Resour. Plann. Manag. 123 (4), 246–249. https://doi.org/10.1061/(ASCE)0733-9496(1997)123:4(246).

Arnosti, C., Jørgensen, B.B., 2003. High activity and low temperature optima of extracellular enzymes in Arctic sediments: implications for carbon cycling by heterotrophic microbial communities. Mar. Ecol. Prog. Ser. 249, 15–24.

Baier, C.T., Purcell, J.E., 1997. Trophic interactions of chaetognaths, larval fish, and zooplankton in the South Atlantic Bight. Mar. Ecol. Prog. Ser. 146, 43–53. https://doi.org/10.3354/meps146043.

Bargu, S., White, J.R., Li, C., Czubakowski, J., Fulweiler, R.W., 2011. Effects of freshwater input on nutrient loading, phytoplankton biomass, and cyanotoxin production in an oligohaline estuarine lake. Hydrobiologia 661 (1), 377–389. https://doi.org/10.1007/s10750-010-0545-8.

Barletta, M., Barletta-Bergan, A., Saint-Paul, U., Hubold, G., 2005. The role of salinity in structuring the fish assemblages in a tropical estuary. J. Fish. Biol. 66, 45–72.

Barron, C.N., Kara, A.B., Martin, P.J., Rhodes, R.C., Smedstad, L.F., 2006. Formulation, implementation and examination of vertical coordinate choices in the global Navy Coastal Ocean Model (NCOM). Ocean Model. 11, 347–375. https://doi.org/10.1016/j.ocemod.2005.01.004.

Bianchi, T.S., DiMarco, S.F., Cowan Jr., J.H., Hetland, R.D., Chapman, P., Day, J.W., Allison, M.A., 2010. The science of hypoxia in the Northern Gulf of Mexico: a review. Sci. Total Environ. 408 (7), 1471–1484. https://doi.org/10.1016/j.scitotenv.2009.11.047.

Brammer, A.J., Rodriguez del Rey, Z., Spalding, E.A., Poirrier, M.A., 2007. Effects of the 1997 Bonnet carre spillway opening on infaunal macroinvertebrates in Lake Pontchartrain, Louisiana. J. Coast. Res. 1292–1303. https://doi.org/10.2112/05-0571.1.

Breitburg, D., 2002. Effects of hypoxia, and the balance between hypoxia and enrichment, on coastal fishes and fisheries. Estuaries 25, 767–781.

Brunner, C.A., Beall, J.M., Bentley, S.J., Furukawa, Y., 2006. Hypoxia hotspots in the Mississippi Bight. J. Foraminifer. Res. 36 (2), 95–107. https://doi.org/10.2113/36.2.95.

Brunner, C.A., Kuykendall, J.I., Hartman, V.A., Howden, S.D., 2008. The impact of hypoxia on foraminifera in the northern Mississippi Bight. Eos Trans. AGU 89, 53, Fall Meet Suppl Abstr OS43C-1306.

Cambazoglu, K.M., Soto, Inia M., Howden, Stephan D., Dzwonkowski, Brian, Fitzpatrick, Patrick J., Arnone, Robert A., Jacobs, Gregg A., Lau, Yee H., 2017. inflow of shelf waters into the Mississippi sound and mobile bay estuaries in october 2015. J. Appl. Remote Sens. 11 (3) https://doi.org/10.1117/1.JRS.11.032410, 032410.

Chakraborty, S., Lohrenz, S.E., 2015. Phytoplankton community structure in the river-influenced continental margin of the northern Gulf of Mexico. Mar. Ecol. Prog. Ser. 521, 31–47. https://doi.org/10.3354/meps11107.

Chappell, B., 2019. Toxic Algae Bloom Closes 25 Beaches On Mississippi's Coast, Fed By Fresh Floodwaters. https://www.npr.org/2019/07/09/739874122/toxic-algae-bloom-closes-25-beaches-on-mississippis-coast-fed-by-fresh-floodwate.

Clark, C., Nnaji, G.A., Huang, W., 2014. Effects of El-Niño and La-Niña sea surface temperature anomalies on annual precipitation and streamflow discharges in southeastern United States. J. Coast. Res. 68 (sp1), 113–120. https://doi.org/10.2112/SI68-015.1.

Cohen, J., Pfeiffer, K., Francis, J., 2017. Winter 2015/16: a turning point in ENSO-based seasonal forecasts. Oceanography 30 (1), 82–89. https://doi.org/10.5670/oceanog.2017.115.

Dalai, T.K., Krishnaswami, S., Sarin, M.M., 2002. Barium in the yamuna River System in the himalaya: sources, fluxes, and its behavior during weathering and transport. G-cubed 3 (12), 1–23. https://doi.org/10.1029/2002GC000381.

Day, J.W., Cable, J.E., Cowan Jr., J.H., DeLaune, R., de Mutsert, K., Fry, B., Mashriqui, H., Justić, D., Kemp, P., Lane, R.R., Rick, J., Rick, S., Rozas, L.P., Snedden, G., Swenson, E., Twilley, R.R., Wissel, B., 2009. The impacts of pulsed reintroduction of river water on a Mississippi delta coastal basin. *J. Coast. Res.*: Special Issue 54, 225–243. https://doi.org/10.2112/SI54-015.1.

DiMarco, S.F., Kelly, F.J., Zhang, J., Guinasso Jr., N.L., 1995. Directional wave spectra on the Louisiana-Texas shelf during Hurricane Andrew. J. Coast. Res. 217–233.

DiMarco, S.F., Meza, E., Zhang, J., 2001. Estimating wave elevation from pressure using second order nonlinear wave-wave interaction theory with applications to Hurricane Andrew. J. Coast. Res. 658–671.

Dortch, Q., Peterson, T., Turner, R.E., 1998. Algal bloom resulting from the opening of the Bonnet Carré spillway in 1997. In: Basics of the Basin Research Symp, 12–13 May. University of New Orleans, New Orleans.

Dortch, M.S., Zakikhani, M., Noel, M.R., Kim, S.C., 2007. Application of a Water Quality Model to Mississippi Sound to Evaluate Impacts of Freshwater Diversions (No. ERDC/EL-TR-07-20). Engineer Research and Development Center, Vicksburg MS, Environmental Lab.

Dzwonkowski, B., Park, K., Jiang, L., 2011. Subtidal across-shelf velocity structure and surface transport effectiveness on the Alabama shelf of the northeastern Gulf of Mexico. J. Geophys. Res. Oceans 116 (C10). https://doi.org/10.1029/2011JC007188.

Dzwonkowski, B., Fournier, S., Park, K., Dykstra, S.L., Reager, J.T., 2018a. Water column stability and the role of velocity shear on a seasonally stratified shelf, Mississippi Bight, northern Gulf of Mexico. J. Geophys. Res. Oceans 123 (8), 5777–5796. https://doi.org/10.1029/2017JC013624.

Dzwonkowski, B., Fournier, S., Reager, J.T., Milroy, S., Park, K., Shiller, A.M., et al., 2018b. Tracking sea surface salinity and dissolved oxygen on a river-influenced, seasonally stratified shelf, Mississippi Bight, northern Gulf of Mexico. Cont Shelf Res 169, 25–33. https://doi.org/10.1016/j.csr.2018.09.009.

Emery, W.J., Thomson, R.E., 2001. Data Analysis Methods in Physical Oceanography, first ed. Elsevier.

Enfield, D.B., 2001. Evolution and historical perspective of the 1997–1998 El niño–southern oscillation event. Bull. Mar. Sci. 69 (1), 7–25.

Fitzpatrick, P., Lau, Y.H., 2018. CONCORDE Meteorological Analysis (CMA) Data Guide, Version 1.0. Geosystems Research Institute, Mississippi State University, Stennis Space Center, MS, p. 23.

Gomez, F.A., Lee, S., Hernandez, F.J., Chiaverano, L.M., Muller-Karger, F.E., Liu, Y., Lamkin, J.T., 2019. ENSO-induced Co-variability of salinity, plankton biomass and coastal currents in the northern Gulf of Mexico. Sci. Rep. 9, 1–10. https://doi.org/10.1038/s41598-018-36655-y.

Gordon, H.R., Wang, M., 1994. Retrieval of water-leaving radiance and aerosol optical thickness over the oceans with Sea-WiFS: a preliminary algorithm. Appl. Optic. 33, 443–452.
Govoni, J., Hoss, D., Chester, A., 1983. Comparative feeding of three species of larval fishes in the Northern Gulf of Mexico: brevoortia patronus, Leiostomus xanthurus, and Micropogonias undulatus. Mar. Ecol. Prog. Ser. 13 (2/3), 189–199. http://www.jstor.org/stable/24815874.
Greer, A.T., Shiller, A.M., Hofmann, E.E., Wiggert, J.D., Warner, S.J., Parra, S.M., et al., 2018. Functioning of COastal River-dominated ecosystems and implications for oil spill response: from observations to mechanisms and models. Oceanography 31 (3), 90–103. https://doi.org/10.5670/oceanog.2018.302.
Guay, C.K., Falkner, K.K., 1997. Barium as a tracer of Arctic halocline and river waters. Deep-Sea Res II 44 (8), 1543–1569. https://doi.org/10.1016/S0967-0645(97)00066-0.
Gundersen, K., Dillon, K., Howden, S., MArtin, K., 2019. River Discharge, Stratification and Shelf Water Hypoxia in the Mississippi Bight. *Estuaries Coasts* (in revisions).
Haidvogel, D.B., Arango, H., Budgell, W.P., Cornuelle, B.D., Curchitser, E., Di Lorenzo, E., Fennel, K., Geyer, W.R., Hermann, A.J., Lanerolle, L., others, 2008. Ocean forecasting in terrain- following coordinates: formulation and skill assessment of the regional ocean modeling system. J. Comput. Phys. 227 https://doi.org/10.1016/j.jcp.2007.06.016, 3,595–3,624.
Hanor, J.S., Chan, L.H., 1977. Non-conservative behavior of barium during mixing of Mississippi River and Gulf of Mexico waters. Earth Planet Sci. Lett. 37 (2), 242–250. https://doi.org/10.1016/0012-821X(77)90169-8.
Harris, R., Wiebe, P., Lenz, J., Skjoldal, H.R., Huntley, M. (Eds.), 2000. ICES Zooplankton Methodology Manual. Elsevier.
Haywood, B.J., White, J.R., Cook, R.L., 2018. Investigation of an early season river flood pulse: carbon cycling in a subtropical estuary. Sci. Total Environ. 635, 867–877. https://doi.org/10.1016/j.scitotenv.2018.03.379.
Hernes, P.J., Spencer, R.G., Dyda, R.Y., Pellerin, B.A., Bachand, P.A., Bergamaschi, B.A., 2008. The role of hydrologic regimes on dissolved organic carbon composition in an agricultural watershed. Geochem. Cosmochim. Acta 72 (21), 5266–5277.
Hillebrand, H., Sommer, U., 1999. The nutrient stoichiometry of benthic microalgal growth: redfield proportions are optimal. Limnol. Oceanogr. 44 (2), 440–446. https://doi.org/10.4319/lo.1999.44.2.0440.
Hillebrand, H., Düruselen, C.D., Kirschetel, D., Pollingher, U., Zohary, T., 1999. Biovolume calculation for pelagic and benthic microalgae. J. Phycol. 35, 403–424.
Ho, P., Shim, M.J., Howden, S.D., Shiller, A.M., 2019. Temporal and spatial distributions of nutrients and trace elements (Ba, Cs, Cr, Fe, Mn, Mo, U, V and Re) in Mississippi coastal waters: influence of hypoxia, submarine groundwater discharge, and episodic events. Cont Shelf Res 175, 53–69. https://doi.org/10.1016/j.csr.2019.01.013.
Holmes Jr., R.R., Watson, K.M., Harris, T.E., 2016. Preliminary Peak Stage and Streamflow Data at Selected U.S. Geological Survey Streamgages for Flooding in the Central and Southeastern United States during December 2015 and January 2016: *U.S.* Geological Survey Open-File Report, 2016–1092, p. 27. https://doi.org/10.3133/ofr20161092.
Hu, C., Feng, L., Lee, Z., Davis, C.O., Mannino, A., McClain, C.R., Franz, B.A., 2012. Dynamic range and sensitivity requirements of satellite ocean color sensors: learning from the past. Appl. Optic. 51 (25), 6045–6062. https://doi.org/10.1364/AO.51.006045.
Huffman, G., 2017. GPM IMERG Final Precipitation L3 1 Month 0.1 Degree X 0.1 Degree V05, Greenbelt, MD, Goddard Earth Sciences Data and Information Services Center (GES DISC). https://doi.org/10.5067/GPM/IMERG/3B-MONTH/05. (Accessed 16 April 2019).
Hunter, J.R., Craig, P.D., Phillips, H.E., 1993. On the use of random walk models with spatially variable diffusivity. J. Comput. Phys. 106, 366–376.
Jacobs, G.A., Huntley, H.S., Kirwan, A.D., Lipphardt, B.L., Campbell, T., Smith, T., Edwards, K., Bartels, B., 2016. Ocean processes underlying surface clustering. J. Geophys. Res. Oceans 121, 180–197. https://doi.org/10.1002/2015JC011140.
Joung, D., Shiller, A.M., 2013. Trace element distributions in the water column near the Deepwater Horizon well blowout. Environ. Sci. Technol. 47 (5), 2161–2168. https://doi.org/10.1021/es303167p.
Joung, D., Shiller, A.M., 2014. Dissolved barium behavior in Louisiana Shelf waters affected by the Mississippi/Atchafalaya River mixing zone. Geochem. Cosmochim. Acta 141, 303–313. https://doi.org/10.1016/j.gca.2014.06.021.
Karmalkar, A.V., Bradley, R.S., 2017. Consequences of global warming of 1.5 C and 2 C for regional temperature and precipitation changes in the contiguous United States. PloS One 12 (1). https://doi.org/10.1371/journal.pone.0168697.
Kesel, R.H., 1988. The decline in the suspended load of the lower Mississippi River and its influence on adjacent wetlands. Environ. Geol. Water Sci. 11 (3), 271–281. https://doi.org/10.1007/BF02574816.
Kolic, P.E., Roy, E.D., White, J.R., Cook, R.L., 2014. Spectroscopic measurements of estuarine dissolved organic matter dynamics during a large-scale Mississippi River flood diversion. Sci. Total Environ. 485, 518–527. https://doi.org/10.1016/j.scitotenv.2014.03.121.
Kong, K., 2017. Southern rockies to northeastern U.S. Winter storm december 26 – 29, 2015. https://origin.wpc.ncep.noaa.gov/storm_summaries/event_reviews/2015/SouthernRockies_Northeast_WinterStorm_Dec2015.pdf. (Accessed 11 February 2019).
Kunkel, K.E., 2003. Sea surface temperature forcing of the upward trend in US extreme precipitation. J. Geophys. Res. Atmos. 108 (D1) https://doi.org/10.1029/2002JD002404. ACL-6.
Lane, R.R., Day Jr., J.W., Kemp, G.P., Demcheck, D.K., 2001. The 1994 experimental opening of the Bonnet Carre spillway to divert Mississippi River water into Lake Pontchartrain, Louisiana. Ecol. Eng. 17 (4), 411–422. https://doi.org/10.1016/S0925-8574(00)00170-1.
Lee, Z., 2014. Update of the quasi-analytical algorithm (QAA_v6). Available online. http://www.ioccg.org/groups/Software_OCA/QAA_v6_2014209.pdf. (Accessed 19 November 2017).
Lee, A., 2019. Bonnet Carré spillway opening is causing a fisheries disaster in Mississippi, governor says, SunHerald. published on June 7. https://www.sunherald.com/news/local/article231300853.html#storylink=cpy.
Lee, Z., Carder, K.L., Arnone, R.A., 2002. Deriving inherent optical properties from water color: a multiband quasi-analytical algorithm for optically deep waters. Appl. Optic. 41, 5755–5772.
Li, W.K.W., 1998. Annual average abundance of heterotrophic bacteria and Synechococcus in surface ocean waters. Limnol. Oceanogr. 7 https://doi.org/10.4319/lo.1998.43.7.1746.
Liefer, J.D., Robertson, A., MacIntyre, H.L., Smith, W.L., Dorsey, C.P., 2013. Characterization of a toxic Pseudo-nitzschia spp. bloom in the Northern Gulf of Mexico associated with domoic acid accumulation in fish. Harmful Algae 26, 20–32. https://doi.org/10.1016/j.hal.2013.03.002.
Liefer, J.D., MacIntyre, H.L., Su, N., Burnett, W.C., 2014. Seasonal alternation between groundwater discharge and benthic coupling as nutrient sources in a shallow coastal lagoon. Estuar. Coast 37 (4), 925–940. https://doi.org/10.1007/s12237-013-9739-4.
Lohrenz, S.E., Fahnenstiel, G.L., Redalje, D.G., Lang, G.A., Chen, X., Dagg, M.J., 1997. Variations in primary production of northern Gulf of Mexico continental shelf waters linked to nutrient inputs from the Mississippi River. Mar. Ecol. Prog. Ser. 155, 45–54. https://doi.org/10.3354/meps155045.
Lopez, J., Henkel, T., Connor, P., 2015. Methodology for Hydrocoast Mapping of the Pontchartrain Basin: 2012 to 2015. Lake Pontchartrain Basin Foundation saveourlake.org. https://saveourlake.org/wp-content/uploads/PDF-Documents/our-coast/Coastal%20Fact%20Sheets/Hydrocoast%20Methodology_Final.pdf.
Marcus, N.H., 2001. Zooplankton: responses to and consequences of hypoxia. In: Rabalais, N.N., Turner, R.E. (Eds.), Coastal Hypoxia: Consequences for Living Resources and Ecosystems, *Coast Estuar Stud*, vol. 58, pp. 49–60.
McConnaughey, J., 2019. NOAA: 279 Dolphins Dead on Gulf Coast, Triple Usual Number. Associated Press. June 14. https://apnews.com/d18ced7257f34d5ba846fa3c08038048.
Mize, S.V., Demcheck, D.K., 2009. Water quality and phytoplankton communities in Lake Pontchartrain during and after the Bonnet Carré spillway opening, April to october 2008, in Louisiana, USA. Geo Mar. Lett. 29 (6), 431–440. https://doi.org/10.1007/s00367-009-0157-3.
Morey, S.L., Martin, P.J., O'Brien, J.J., Wallcraft, A.A., Zavala-Hidalgo, J., 2003. Export pathways for river discharged fresh water in the northern Gulf of Mexico. J. Geophys. Res. Oceans 108 (C10). https://doi.org/10.1029/2002JC001674.
Mossa, J., 1996. Sediment dynamics in the lowermost Mississippi River. Eng. Geol. 45 (1–4), 457–479. https://doi.org/10.1016/S0013-7952(96)00026-9.
Newton, A., 2019. 'They're all dead:' Mississippi oyster farms take hit from Bonnet Carre Spillway. Sun. Herald. June 12. https://www.sunherald.com/news/local/article231492933.html.
NOAA National Centers for Environmental Information, 2016. State of the climate: national climate Report for december 2015. https://www.ncdc.noaa.gov/sotc/national/201512. (Accessed 12 April 2019).
O'Reilly, J.E., Maritorena, S., Mitchell, B.G., Siegel, D.A., Carder, K.L., Garver, S.A., Kahru, M., McClain, C., 1998. Ocean color chlorophyll algorithms for SeaWiFS. J. Geophys. Res. Oceans 103 (C11), 24937–24953. https://doi.org/10.1029/98JC02160.
Officer, C.B., Ryther, J.H., 1980. The possible importance of silicon in marine eutrophication. Mar. Ecol. Prog. Ser. 3, 83–91.
Ondrusek, M., Lance, V.P., 2015. Report for Dedicated JPSS VIIRS Ocean Color Calibration/Validation Cruise, vol. 146. NOAA Technical Report NESDIS. https://doi.org/10.7289/V52B8W0Z.
Paerl, H.W., 1996. A comparison of cyanobacterial bloom dynamics in freshwater, estuarine and marine environments. Phycologia 35 (Suppl. 6), 25–35. https://doi.org/10.2216/i0031-8884-35-6S-25.1.
Parra, S.M., Greer, A.T., Book, J.W., Deary, A.L., Soto, I.M., Culpepper, C., Hernandez, F. J., Miles, T.N., 2019. Acoustic detection of zooplankton diel vertical migration behaviors on the northern Gulf of Mexico shelf. Limnol. Oceanogr. 64 (5), 2092–2113. https://doi.org/10.1002/lno.11171.
Pegau, W.S., Gray, D., Zaneveld, J.R.V., 1997. Absorption and attenuation of visible and near-infrared light in water: dependence on temperature and salinity. Appl. Optic. 36 (24), 6035–6046. https://doi.org/10.1364/ao.36.006035.
Perkins, H., de Strobel, F., Gualdesi, L., 2000. The Barny sentinel trawl-resistant ADCP bottom mount: design, testing, and application. IEEE J. Ocean. Eng. 25 (4), 430–436. https://doi.org/10.1109/48.895350.
Perret, W.S., Warren, J., Buchanan, M., Engel, L., 1997. Monitoring and assessment of the 1997 Bonnet Carré Spillway opening in Mississippi Sound. Contract Number WAS-S-0497–0261 Completion Report.
Posadas, B.C., Posadas, B.K.A., 2017. Economic impacts of the opening of the Bonnet carre spillway to the Mississippi oyster fishery. J. Food Distrib. Res. 48 (856-2018-3072).
Purcell, J.E., Breitburg, D.L., Decker, M.B., Graham, W.M., Youngbluth, M.J., Raskoff, K. A., 2001. Pelagic Cnidarians and ctenophores in low dissolved oxygen environments: a review. In: Rabalais, N.N., Turner, R.E. (Eds.), Coastal Hypoxia: Consequences for Living Resources and Ecosystems. American Geophysical Union, Washington, DC, pp. 77–100.
Qian, Y., Jochens, A.E., Kennicutt Ii, M.C., Biggs, D.C., 2003. Spatial and temporal variability of phytoplankton biomass and community structure over the continental margin of the northeast Gulf of Mexico based on pigment analysis. Cont Shelf Res 23 (1), 1–17. https://doi.org/10.1016/S0278-4343(02)00173-5.

Rabalais, N.N., Turner, R.E., Wiseman Jr., W.J., 2002. Gulf of Mexico hypoxia, aka "The dead zone". Annu. Rev. Ecol. Systemat. 33 (1), 235–263. https://doi.org/10.1146/annurev.ecolsys.33.010802.150513.

Rabalais, N.N., Turner, R.E., Sen Gupta, B.K., Boesch, D.F., Chapman, P., Murrell, M.C., 2007. Characterization and long-term trends of hypoxia in the northern Gulf of Mexico: does the science support the Action Plan. Estuar. Coast 30 (5), 753–772. https://doi.org/10.1007/BF02841332.

Redfield, A.C., 1958. The biological control of chemical factors in the environment. Am. Sci. 46 (3), 230A-221.

Roesler, C.S., Barnard, A.H., 2013. Optical proxy for phytoplankton biomass in the absence of photophysiology: rethinking the absorption line height. Methods Oceanogr. 7, 79–94. https://doi.org/10.1016/j.mio.2013.12.003.

Röttgers, R., McKee, D., Woźniak, S.B., 2013. Evaluation of scatter corrections for ac-9 absorption measurements in coastal waters. Methods Oceanogr. 7, 21–39. https://doi.org/10.1016/j.mio.2013.11.001.

Roy, E.D., White, J.R., 2012. Nitrate flux into the sediments of a shallow oligohaline estuary during large flood pulses of Mississippi River water. J. Environ. Qual. 41 (5), 1549–1556. https://doi.org/10.2134/jeq2011.0420.

Roy, E.D., White, J.R., Smith, E.A., Bargu, S., Li, C., 2013. Estuarine ecosystem response to three large-scale Mississippi River flood diversion events. Sci. Total Environ. 458, 374–387. https://doi.org/10.1016/j.scitotenv.2013.04.046.

Roy, E.D., Smith, E.A., Bargu, S., White, J.R., 2016. Will Mississippi River diversions designed for coastal restoration cause harmful algal blooms? Ecol. Eng. 91, 350–364.

Roy, E.D., Nguyen, N.T., White, J.R., 2017. Changes in estuarine sediment phosphorus fractions during a large-scale Mississippi River diversion. Sci. Total Environ. 609, 1248–1257. https://doi.org/10.1016/j.scitotenv.2017.07.224.

Rubin-Oster, B., 2017. Western and central U.S. Winter storm – 13-16 december, 2015. https://origin.wpc.ncep.noaa.gov/storm_summaries/event_reviews/2015/Western_Central_US_WinterStorm_Dec2015.pdf. (Accessed 11 February 2019).

Sanchez-Rubio, G., Perry, H.M., Biesiot, P.M., Johnson, D.R., Lipcius, R.N., 2011. Oceanic–atmospheric modes of variability and their influence on riverine input to coastal Louisiana and Mississippi. J. Hydrol. 396 (1–2), 72–81. https://doi.org/10.1016/j.jhydrol.2010.10.034.

Sanial, V., Shiller, A.M., Joung, D., Ho, P., 2019. Extent of Mississippi River water in the Mississippi Bight and Louisiana Shelf based on water isotopes. Estuar. Coast Shelf Sci. 226, 106196. https://doi.org/10.1016/j.ecss.2019.04.030.

Santorelli, A., 2016. Central Plains to upper Great lakes winter storm 20-22 november, 2015. https://origin.wpc.ncep.noaa.gov/storm_summaries/event_reviews/2015/CentralPlains_UpperLakes_WinterStorm_Nov2015.pdf. (Accessed 11 February 2019).

Schiller, R.V., Kourafalou, V.H., Hogan, P., Walker, N.D., 2011. The dynamics of the Mississippi River plume: impact of topography, wind and offshore forcing on the fate of plume waters. J. Geophys. Res. Oceans 116 (C6). https://doi.org/10.1029/2010JC006883.

Shchepetkin, A.F., McWilliams, J.C., 2005. The regional oceanic modeling system (ROMS): a split-explicit, free-surface, topography- following-coordinate oceanic model. Ocean Model. 9, 347–404. https://doi.org/10.1016/.j.ocemod.2004.08.002.

Shim, M.J., Swarzenski, P.W., Shiller, A.M., 2012. Dissolved and colloidal trace elements in the Mississippi River delta outflow after Hurricanes Katrina and Rita. Cont Shelf Res 42, 1–9. https://doi.org/10.1016/j.csr.2012.03.007.

Sieracki, C.K., Sieracki, M.E., Yentsch, C.S., 1998. An imaging-in-flow system for automated analysis of marine microplankton. Mar. Ecol. Prog. Ser. 168, 285–296. https://doi.org/10.3354/meps168285.

Stumpf, R.P., Gelfenbaum, G., Pennock, J.R., 1993. Wind and tidal forcing of a buoyant plume, Mobile Bay, Alabama. Cont Shelf Res 13 (11), 1281–1301. https://doi.org/10.1016/0278-4343(93)90053-Z.

Templet, P.H., Meyer-Arendt, K.J., 1988. Louisiana wetland loss: a regional water management approach to the problem. Environ. Manag. 12 (2), 181–192. https://doi.org/10.1007/BF01873387.

Turner, R.E., Qureschi, N., Rabalais, N.N., Dortch, Q., Justić, D., Shaw, R.F., Cope, J., 1998. Fluctuating silicate:nitrate ratios and coastal food webs. Proc. Natl. Acad. Sci. U.S.A. 95, 13048–13051.

Turner, R.E., Dortch, Q., Rabalais, N.N., 2004. Inorganic nitrogen transformations at high loading rates in an oligohaline estuary. Biogeochemistry 68 (3), 411–423. https://doi.org/10.1023/B:BIOG.0000031039.56794.29.

USACE, 1945. Stages and Discharges Mississippi River and It's Outlets and Tributaries 1945. Mississippi River Commission, p. 145.

USACE, 1950. Stages and Discharges of Mississippi River and It's Outlets and Tributaries 1950. Office of the President, Mississippi River Commission, Army-MRC, Vicksburg, MS.

USACE, 1974. Flood of '73, Post-Flood Report, vol. I. New Orleans District. U. S. Army Corps of Engineers, New Orleans, LA, p. 391.

USACE, 1975. Flood of '75, Post-Flood Report. New Orleans District. U. S. Army Corps of Engineers, New Orleans, LA, p. 185.

USACE, 1980. Flood of '79, Post-Flood Report. New Orleans District. U. S. Army Corps of Engineers, New Orleans, LA, p. 210.

USACE, 1984. Flood of '83, Post-Flood Report. U. S. Army Corps of Engineers, New Orleans District, P.O. Box 60267, New Orleans, LA. 70160, April 1984, p. 162.

USACE, 2019. Spillway Operation Information. https://www.mvn.usace.army.mil/Missions/Mississippi-River-Flood-Control/Bonnet-Carre-Spillway-Overview/Spillway-Operation-Information/. (Accessed 19 August 2019).

van Geldern, R., Barth, J.A., 2012. Optimization of instrument setup and post-run corrections for oxygen and hydrogen stable isotope measurements of water by isotope ratio infrared spectroscopy (IRIS). Limnol Oceanogr. Methods 10 (12), 1024–1036. https://doi.org/10.4319/lom.2012.10.1024.

Visser, A.W., 1997. Using random walk models to simulate the vertical distribution of particles in a turbulent water column. Mar. Ecol. Prog. Ser. 158, 275–281.

Vu, V.Q., 2011. ggbiplot: a ggplot2 based biplot. R package version 0.55. http://github.com/vqv/ggbiplot.

Wagner, A.J., Slowey, N.C., 2011. Oxygen isotopes in seawater from the Texas-Louisiana Shelf. Bull. Mar. Sci. 87 (1), 1–12. https://doi.org/10.5343/bms.2010.1004.

Walker, N.D., 1996. Satellite assessment of Mississippi River plume variability: causes and predictability. Remote Sens. Environ. 58 (1), 21–35. https://doi.org/10.1016/0034-4257(95)00259-6.

Walker, N.D., Wiseman Jr., W.J., Rouse Jr., L.J., Babin, A., 2005. Effects of river discharge, wind stress, and slope eddies on circulation and the satellite-observed structure of the Mississippi River plume. J. Coastal. Res. 1228–1244. https://doi.org/10.2112/04-0347.1.

War Department, Corps of Engineers, U. S. Army, 1937. Daily discharge of Mississippi river and its tributaries and outlets 1937. Office of the president, *Mississippi river commission*, vicksburg, MS. M.R.C. Print 750, 9–41.

Warner, John, Armstrong, Brandy, He, Ruoying, Zambon, Joseph, 2010. Development of a Coupled Ocean-Atmosphere-Wave-Sediment transport (COASWST) modeling system. Ocean Model. 35, 230–244. https://doi.org/10.1016/j.ocemod.2010.07.010.

Welschmeyer, N.A., 1994. Fluorometric analysis of chlorophyll a in the presence of chlorophyll b and pheopigments. Limnol. Oceanogr. 39 (8), 1985–1992. https://doi.org/10.4319/lo.1994.39.8.1985.

Werdell, P.J., Franz, B.A., Bailey, S.W., Feldman, G.C., et al., 2013. Generalized ocean color inversion model for retrieving marine inherent optical properties. Appl. Optic. 52, 2019–2037.

Weston, N.B., Joye, S.B., 2005. Temperature-driven decoupling of key phases of organic matter degradation in marine sediments. Proc. Natl. Acad. Sci. Unit. States Am. 102 (47), 17036–17040.

WETLabs, 2011. AC Meter Protocol Document. AC Meter Protocol (Acprot). Revision Q 20 April 2011.

Wuebbles, D.J., Hayhoe, K., 2004. Climate change projections for the United States Midwest. Mitig. Adapt. Strategies Glob. Change 9 (4), 335–363. https://doi.org/10.1023/B:MITI.0000038843.73424.de.